

## Article

# Single-Shunt Three-Phase Current Measurement for a Three-Level Inverter Using a Modified Space-Vector Modulation

Haris Kovačević <sup>1,\*</sup>, Lucijan Korošec <sup>2</sup> and Miro Milanovič <sup>3</sup> <sup>1</sup> Emsiso d.o.o., 2211 Pesnica pri Mariboru, Slovenia<sup>2</sup> Mahle Electric Drives Slovenija d.o.o., 5290 Šempeter pri Gorici, Slovenia; korossec@gmail.com<sup>3</sup> Faculty of Electrical Engineering and Computer Science, University of Maribor, 2000 Maribor, Slovenia; miro.milanovic@um.si

\* Correspondence: hariskovacevi@gmail.com

**Abstract:** This article presents a single-shunt measurement of a three-level inverter using a modified space-vector modulation to reconstruct the three-phase load current. The proposed method was implemented on a digital signal processor (DSP), and the algorithm was verified in the laboratory experiment. Through the work, it was proven that the single-shunt three-phase current measurement could be performed using the space-vector modulation for three-level inverters in an analogous way to ordinary three-phase inverters. Three-phase current reconstruction for ordinary three-phase inverters was performed using the ordinary space-vector modulation with eight vectors, but for three-level inverters, 21 vectors were available. When the inverter was working on the edges between two vectors, the modulation disturbances appeared as current spikes. This problem was solved using the modified SVM performed by shifting the SVM signals. Carefully designed signal shifting (vector injection) demonstrated an excellent reconstruction of the three-phase load currents that were single-shunt measured.

**Keywords:** single shunt; three-level inverter; SVM modification; current reconstruction; vector injection



check for updates

**Citation:** Kovačević, H.; Korošec, L.; Milanovič, M. Single-Shunt Three-Phase Current Measurement for a Three-Level Inverter Using a Modified Space-Vector Modulation. *Electronics* **2021**, *10*, 1734. <https://doi.org/10.3390/electronics10141734>

Academic Editor: Ahmed Abu-Siada

Received: 9 June 2021

Accepted: 16 July 2021

Published: 19 July 2021

**Publisher's Note:** MDPI stays neutral with regard to jurisdictional claims in published maps and institutional affiliations.



**Copyright:** © 2021 by the authors. Licensee MDPI, Basel, Switzerland. This article is an open access article distributed under the terms and conditions of the Creative Commons Attribution (CC BY) license (<https://creativecommons.org/licenses/by/4.0/>).

## 1. Introduction

Inverters are used widely for motor control applications that are based on performance, control principles, motor type, etc. [1–3]. Considering control principles, motor drives can be divided into two groups: scalar- and vector-modulated, and controlled motor drives. Scalar modulations are used in applications such as conveyor belts, passenger elevators, grinders, etc. [3]. The main advantage of scalar control is its simplicity [1,2], and it is usually used in low-cost and low-performance drives [1]. Vector control is usually applied for applications in which better dynamic responses and high performances are required [4]. Two-level inverters are usually used, due to their simplicity, price, high reliability, and performance. Introducing the multilevel architecture into the inverter's operation principle reduces the harmonic distortion and switching stress in the inverter circuit. Different topologies have been reported for multilevel inverters, such as diode-clamped (neutral clamped) inverters [5,6], capacitor-clamped (flying capacitors) inverters [7,8], and cascaded multicell inverters with a separate DC source [7,9]. Diode-clamped inverters split the DC-link voltage into  $n$  levels by  $n-1$  series-connected bulk capacitors, where the middle point between the two capacitors is called a neutral point. Two additional diodes clamp the switch voltage to  $n-1$ , the level of the DC-link voltage. Capacitor-clamped inverters use independent capacitors to clamp the device voltage. Cascaded multicell inverters consist of a series connection of single-phase inverters with separate DC sources. With such topology, the resulting phase voltage is equal to the sum of the voltages generated by the different cells.

To reduce the costs of a device, a single-shunt measurement can be used instead of current measurement using two or three shunts (or hall sensors). In addition, this

measurement principle can be implemented for safety reasons as a second (redundant) measurement system. To achieve this, space-vector modulation must be modified, since the current measurement inside the boundary area (between two vectors) is not accurate enough when ordinary space-vector modulation is used. When using the single-shunt current measurement, it shall be considered that the switching stress, harmonic distortion, DC link voltage utilization, and current measurement accuracy are adequate. Two switch events are desired from a switching stress point of view. Symmetric SVM signals are desired from the harmonic distortion, DC link voltage utilization, and current measurement points of view. In such case, the average current value occurs in the middle of the time interval between the two SVM edges.

Several different methods have been identified to achieve this for three-level inverters [10–19]. Due to the hardware limitations of the current-measuring circuits, accurate current measurement is not possible while an arbitrary voltage vector is positioned close to the sector boundary [13–15] or region boundary inside the vector's diagram of three-level inverters [19,20] by using ordinary space-vector modulation. Current measurement inside a boundary area is solved most often using modification algorithms based on SVM signal shifting [21], which are not often used for multilevel inverters, or additional voltage vector injection [22–24]. Paper [20] presents an estimation algorithm in combination with vector injection, used to solve a problem with boundary areas while only one current measurement is possible. A predictive algorithm [25], a hybrid solution combined with space-vector modulation and the SVM method [26], and current reconstruction strategy with online current offset compensation [27] could also be used for a single-shunt current-measurement approach. A tristate pulse-width modulation technique for single-shunt current reconstruction could be used when hardware and software resources are limited [28]. By proper design of the current measurement circuit, DC link voltage utilization could improve drastically. There are several papers that describe different approaches for current-measurement circuit design [29,30].

This paper deals with the development of a modified space-vector modulation (SVM) to reconstruct the three-phase load current by using the single-shunt measurement. The proposed method is based on the algorithms developed for two-level inverter circuits, presented in [13–16]. To solve a problem with boundary areas, SVM signals have been shifted in order to reduce additional vector injection. Section 2 describes the basic operation of a three-level DC–AC converter, and proposes SVM patterns to achieve space vector modulation. Such organized modulation principle suffers with inaccuracy on the vector's boundaries, so the modified SVM patterns enable the single-shunt current measurements inside the boundary areas. For this reason, the SVM signals were shifted, as is discussed in Section 3. The three-level DC–AC converter's design is described in Section 4. Section 5 deals with experimental verification of the proposed single-shunt space-vector modulation approach.

## 2. Three-Level Inverter Basics

A basic schematic of the three-level inverter is shown in Figure 1. Each phase consists of four MOSFETs and two bypass diodes. To avoid a possible short circuit, three switching states are allowed for each phase (leg), as shown in Table 1. With different combinations of switching states in each phase, 27 basic voltage vectors can be produced. Three of them represent the zero vectors.

A vector diagram for the three-level inverter is shown in Figure 2a. Vectors  $\vec{V}_1 - \vec{V}_6$ , if drawn with the start point in the reference frame origin, form an inner hexagon with their vector end. Such vectors can be achieved using two different combinations of switching states.

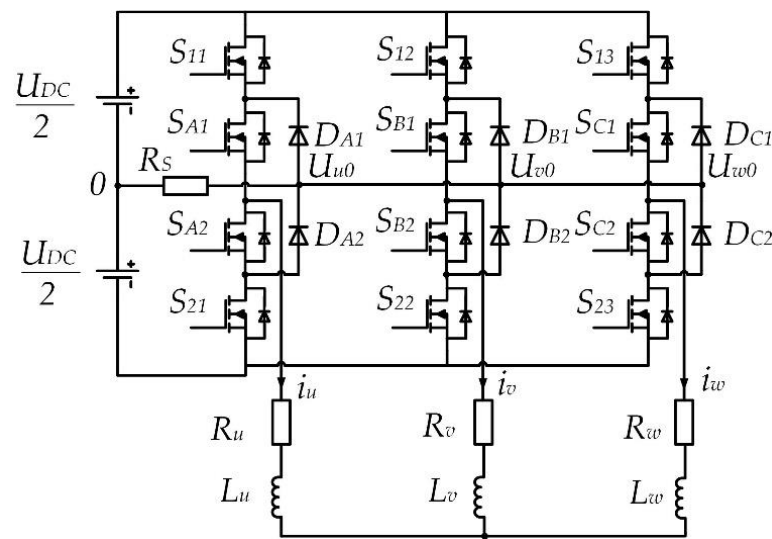


Figure 1. Schematic of a three-level DC-AC converter.

Table 1. Switching states of a three-level DC-AC converter.

$S_{1x}$	$S_{x1}$	$S_{x2}$	$S_{2x}$	$U_{x0}$	Notation
1	1	0	0	$U_{DC}/2$	P
0	1	1	0	0	0
0	0	1	1	$-U_{DC}/2$	N

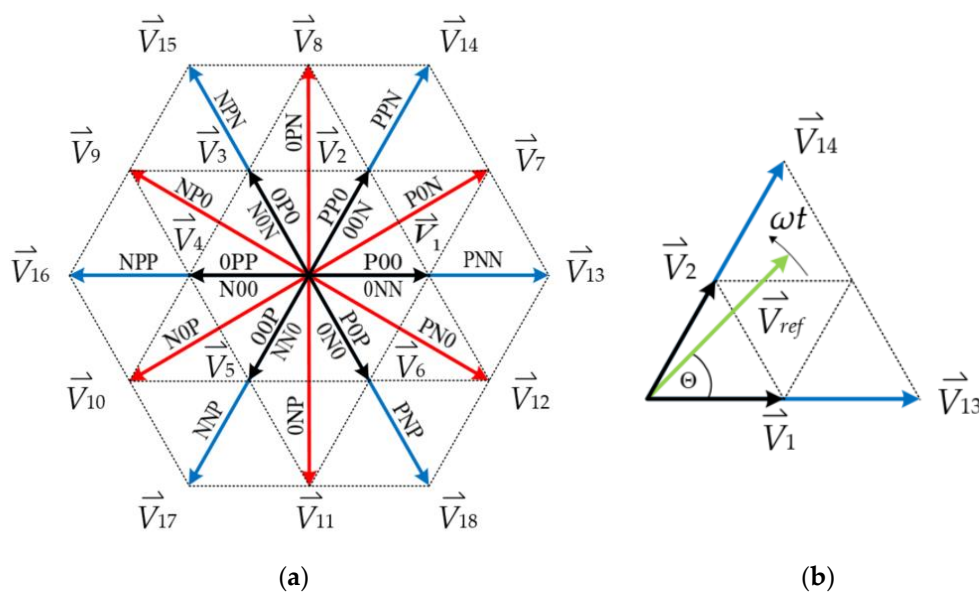


Figure 2. (a) Vector diagram for a three-level inverter; (b) reference voltage vector positioned in the first sector.

Vectors  $\vec{V}_7 - \vec{V}_{18}$  form an outer hexagon with their vector end. The outer hexagon can be divided into six sectors, which are areas inside the hexagon shifted by  $60^\circ$  and starting from  $0^\circ$ . Each sector inside the vector diagram can be divided into four triangular areas called regions. Space-vector modulation for a three-level inverter can be achieved by applying a different SVM pattern for each region formed from the three nearest basic voltage vectors. With such an approach, the SVM pattern for each region is symmetric.

The modulation index for the three-level DC-AC converter can be calculated as follows:

$$m_i = \sqrt{3} \cdot \frac{U_{ref}}{U_{DC}} \tag{1}$$

where  $U_{ref}$  represents the reference voltage vector length and  $U_{DC}$  represents the DC link voltage. To determine a region, the modulation index components shall be determined as follows:

$$m_{i,x} = \sqrt{3} \cdot \frac{U_{ref}}{U_{DC}} \sin(60^\circ - \theta) \tag{2}$$

$$m_{i,y} = \sqrt{3} \cdot \frac{U_{ref}}{U_{DC}} \sin(\theta) \tag{3}$$

where  $\theta$  stands for the reference voltage vector angle transferred to Sector 1. The reference voltage vector positioned in the first sector is shown in Figure 2b. Based on the modulation index components, the region is determined as shown in Table 2.

**Table 2.** Region decision.

$m_{i,x}$	$m_{i,y}$	$m_{i,x} + m_{i,y}$	Region
<0.5	<0.5	<0.5	1
<0.5	<0.5	>0.5	2
>0.5	-	-	3
-	>0.5	-	4

The first sector is divided into four regions, as shown in Figure 3. An arbitrary voltage vector can be generated with linear combination of two or more basic voltage vectors and null vectors. To keep the SVM switching pattern symmetric, two or three nearest basic voltage vectors in combination with or without null vectors are used for each region.

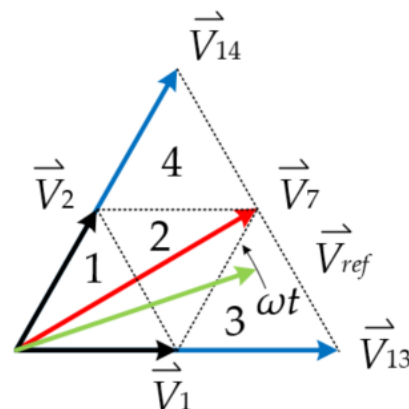


**Figure 3.** First sector divided into regions.

The reference voltage vector shown in Figure 3 is positioned inside Region 3. With linear combination of the nearest vectors  $\vec{V}_1$ ,  $\vec{V}_7$ , and  $\vec{V}_{13}$ , the reference voltage vector can be achieved as follows:

$$\vec{V}_{ref} = \vec{V}_1 + \vec{V}_7 + \vec{V}_{13} \tag{4}$$

Controlling the duration of the basic voltage vectors  $\vec{V}_1$ ,  $\vec{V}_7$ , and  $\vec{V}_{13}$ , a reference voltage vector can be generated anywhere inside Region 3. Expressions for the basic voltage vector length calculation inside Sector 1 are shown in Table 3.

In an equivalent way, a time calculation can be done for other regions using different linear vector combinations. Table 4 shows the time calculations for all regions inside Sector 1. Transferring the reference voltage vector to the first sector, the same expression from Table 4 can be applied to other sectors. The SVM patterns of all sectors and regions are presented in Figure 4. The vector sequence and current-sampling positions are shown for each SVM pattern. Current-sampling positions are marked with colored arrows in Figure 4, where a red arrow marks the first sampling point, a blue arrow marks the second sampling point, and a green arrow marks the third sampling point only in Region 2, due to



the fact that all three phase currents can be measured within a switching period, which will be explained in the next section. The time calculation for Region 3 can be obtained using Expression (4). In an equivalent way, a time calculation can be done for other regions using different linear vector combinations. Table 4 shows the time calculations for all regions inside Sector 1.

**Table 3.** Basic voltage vectors used inside Sector 1.

Voltage Vector	Duty Cycle	Expression
$\vec{V}_1$	$d_1 = \frac{1}{3} \frac{t_1}{T_s}$	$d_1 \cdot U_{DC} \cdot e^{j0}$
$\vec{V}_2$	$d_2 = \frac{1}{3} \frac{t_2}{T_s}$	$d_2 \cdot U_{DC} \cdot e^{j\frac{\pi}{3}}$
$\vec{V}_7$	$d_7 = \frac{1}{\sqrt{3}} \frac{t_0}{T_s}$	$d_7 \cdot U_{DC} \cdot e^{j\frac{\pi}{6}}$
$\vec{V}_{13}$	$d_{13} = \frac{2}{3} \frac{t_2}{T_s}$	$d_{13} \cdot U_{DC} \cdot e^{j0}$
$\vec{V}_{14}$	$d_{14} = \frac{2}{3} \frac{t_1}{T_s}$	$d_{14} \cdot U_{DC} \cdot e^{j\frac{\pi}{3}}$
$\vec{V}_0$	$d_0 = \frac{t_0}{T_s}$	$0 \cdot d_0 \cdot U_{DC}$

**Table 4.** Time calculation for different regions.

Region	$t_1$	$t_2$	$t_0$
1	$t_1 = 2 \cdot m_i \cdot T_s \cdot \sin(60^\circ - \theta)$	$t_2 = 2 \cdot m_i \cdot T_s \cdot \sin(\theta)$	$t_0 = T_s - t_1 - t_2$
2	$t_1 = T_s \cdot (1 - 2 \cdot m_i \cdot \sin(\theta))$	$t_2 = T_s \cdot (1 - 2 \cdot m_i \cdot \sin(60^\circ - \theta))$	$t_0 = T_s - t_1 - t_2$
3	$t_1 = T_s - t_2 - t_0$	$t_2 = T_s \cdot (2 \cdot m_i \cdot \sin(60^\circ - \theta) - 1)$	$t_0 = 2 \cdot m_i \cdot T_s \cdot \sin(\theta)$
4	$t_1 = T_s \cdot (2 \cdot m_i \cdot \sin(\theta) - 1)$	$t_2 = T_s - t_1 - t_0$	$t_0 = 2 \cdot m_i \cdot T_s \cdot \sin(60^\circ - \theta)$

To take a sample of current measurement during a switching period at the right moment, the active basic voltage vector needs to be known. Based on that, it can be determined which phase current is measured. When the values of two-phase currents are known, we can determine the third phase current easily. Figure 5 presents the described current reconstruction principle shown for Sector 1 and Region 1, where the first current sample is measured during vector  $\vec{V}_1$  and the second current sample is measured during vector  $\vec{V}_2$ . At a certain time instant, the instantaneous value of current  $i_v$  is sampled and multiplied by  $(-1)$ , and at the next time instant, the instantaneous value of current  $i_u$  is sampled. Table 5 shows which current is measured for each basic voltage vector. As can be seen, the current measurement is not possible to perform for basic voltage vectors  $\vec{V}_{13} - \vec{V}_{18}$ , since the current is not flowing through the shunt resistor, therefore the third current  $i_u$  is determined using Kirchoff’s current law.

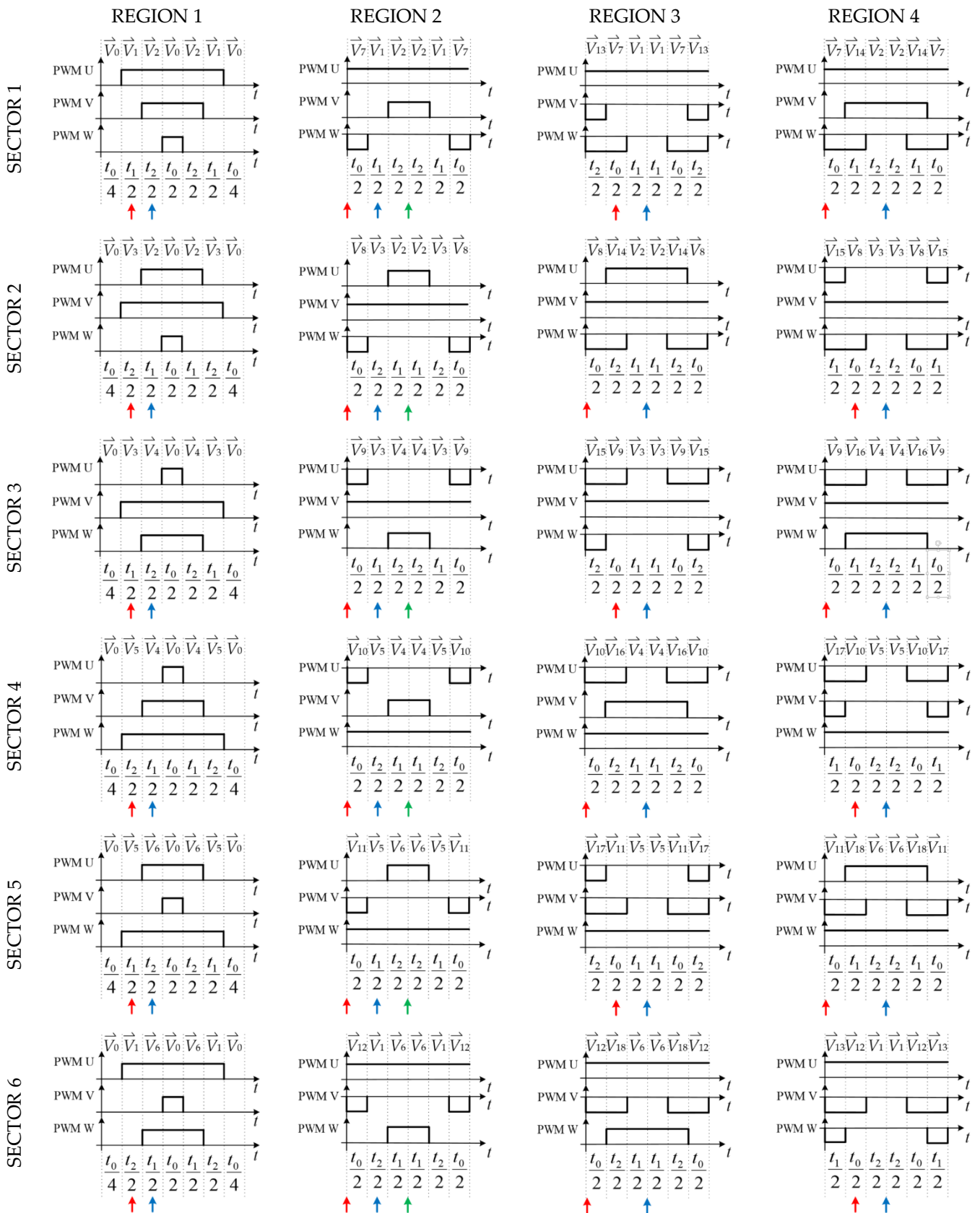


Figure 4. Proposed SVM patterns.

**Table 5.** Current measurement.

Voltage Vector	Switching State	Current Measurement
$\vec{V}_1$	P00 0NN	$I_u$ $-I_u$
$\vec{V}_2$	PP0 00N	$-I_w$ $I_w$
$\vec{V}_3$	OP0 NON	$I_v$ $-I_v$
$\vec{V}_4$	OPP N00	$-I_u$ $I_u$
$\vec{V}_5$	0OP NN0	$I_w$ $-I_w$
$\vec{V}_6$	POP 0N0	$-I_v$ $I_v$
$\vec{V}_7$	P0N	$-I_v$
$\vec{V}_8$	OPN	$-I_u$
$\vec{V}_9$	NP0	$-I_w$
$\vec{V}_{10}$	N0P	$-I_v$
$\vec{V}_{11}$	ONP	$-I_u$
$\vec{V}_{12}$	PN0	$-I_w$
$\vec{V}_{13}$	PNN	-
$\vec{V}_{14}$	PPN	-
$\vec{V}_{15}$	NPN	-
$\vec{V}_{16}$	NPP	-
$\vec{V}_{17}$	NNP	-
$\vec{V}_{18}$	PNP	-

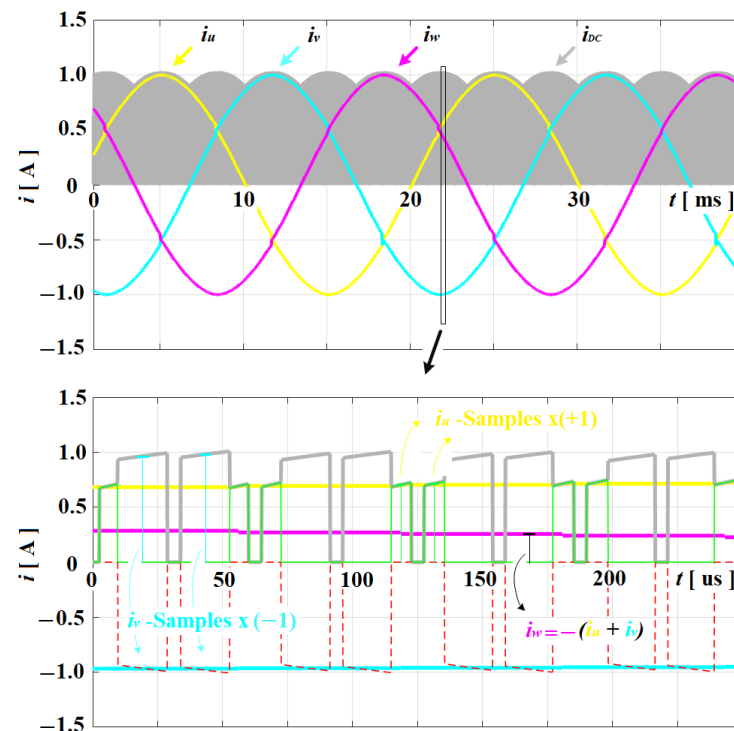


Figure 5. Current reconstruction.

### 3. Proposed SVM Pattern-Modification Method

As previously described in Section 2, two current samples are measured inside a switching period between two SVM edges. The problem occurs when the time between the two SVM edges becomes too short for current measurement due to the hardware limitation and measurement signal settling time, described in [4–8]. The time between two SVM edges becomes too short if the arbitrary voltage vector is close to the sector or region boundaries. Such critical areas are shown in Figure 6.

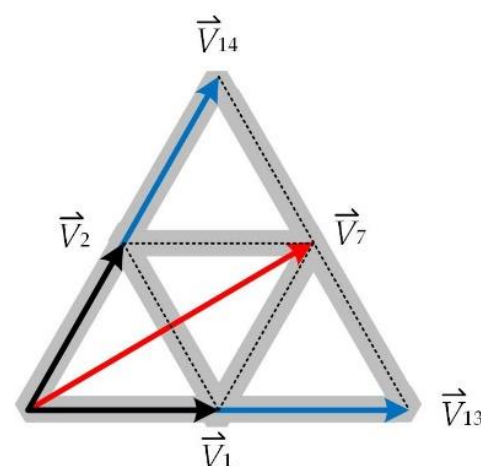


Figure 6. Boundary areas for the first sector.

In such boundary cases, the conventional method from Section 2 cannot serve for the single-shunt current-measurement approach, since current samples cannot be taken twice within a switching period, and can only be used inside a normal operating area. Different methods are proposed for solving boundary-area problems in the literature [3–15]. Most of the proposed methods use the vector-injection approach. While injecting additional vectors, asymmetry to the SVM pattern is introduced, which will cause higher current

ripple and negative impact to the harmonic distortion at the end. There is also an additional problem with current measurement precision using asymmetric SVM signals, as the average current value may occur in different positions between two SVM edges, which requires a more complex calculation to determine the correct sampling time. Without that, it could happen that a current ripple is measured instead of the average current. To overcome these problems, the proposed method for boundary areas reduces vector injection to the minimum. This method uses SVM shifting, like the classic method for two-level inverters. The SVM-shifting method differs for different regions, where the basic idea is to shift one or more SVM signals to ensure enough time for current measurement, which will be explained later in this section. Boundary-area design is determined with a minimum time window for current measurement [3–5]. With proper boundary-area design, two current samples can be measured inside the whole boundary area. Using the proposed method, all three-phase currents can be measured inside Region 2, which reduces vector injection and avoids SVM shifting.

### 3.1. SVM Pattern Modification Inside Region 1

Figure 7a shows Region 1 inside Sector 1, divided into a few characteristics areas: normal operating area, boundary area 1, boundary area 2, and an unreachable area. With the linear combination of the basic voltage vectors  $\vec{V}_1$  and  $\vec{V}_2$ , an arbitrary voltage vector is obtained, as also shown in Figure 7a.

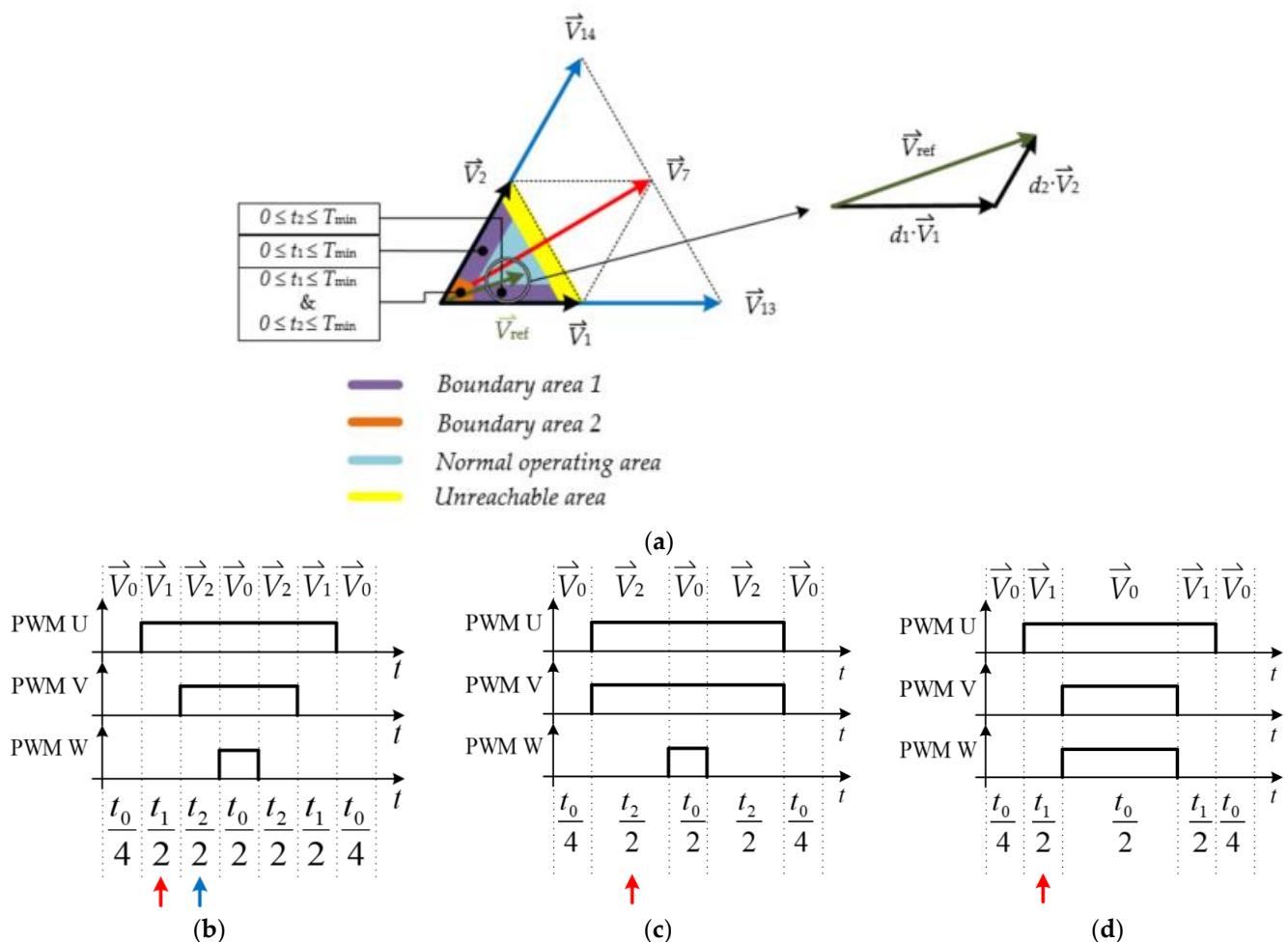


**Figure 7.** (a) Vector diagram for Sector 1 and Region 1 with marked problematic areas for single-shunt measurement; (b) SVM pattern for Sector 1 and Region 1 inside the normal operating area; (c) SVM pattern while  $t_1 = 0$  s; (d) SVM pattern while  $t_2 = 0$  s.

The SVM pattern for a normal operating area is shown in Figure 7b. Inside the normal operating area, time durations  $t_1$  and  $t_2$  are long enough for accurate current measurement between two SVM edges. The time duration is long enough if it is longer than  $T_{min}$ , which depends on the hardware design, deadtime, and settling time. Reducing time  $T_{min}$ , the unreachable area is reduced, and a larger arbitrary voltage vector can be generated. It is desired that  $T_{min}$  is as short as possible.

Moving close to the boundary area, the time between two SVM edges becomes shorter than  $T_{min}$ . In such a case, there is not enough time for current measurement, due to the hardware limitations. Figure 7c shows the case in which the arbitrary voltage vector is aligned with the basic voltage vector  $\vec{V}_1$ . In such a case, time  $t_2$  is equal to zero, and current measurement is only possible during vector  $\vec{V}_1$ , which is not enough for current reconstruction. An analogous situation is shown in Figure 7d, in which the arbitrary voltage vector is aligned with basic voltage vector  $\vec{V}_2$ . In such case, time  $t_1$  is equal to zero and current measurement is only possible during vector  $\vec{V}_2$ .

To overcome a problem with current measurement while the arbitrary voltage vector is inside the boundary area 1 in Region 1, the SVM modification pattern is proposed, as shown in Figure 8a,b.

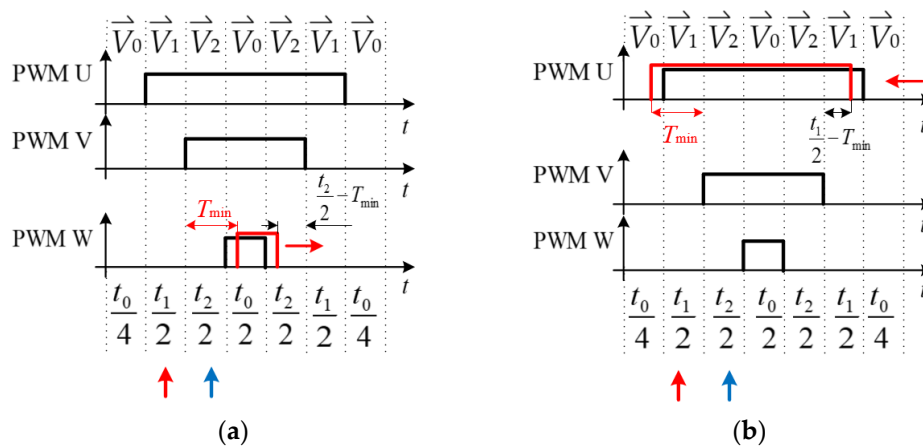


Figure 8. (a) SVM modification pattern while  $t_2 < T_{min}$ ; (b) SVM modification pattern while  $t_1 < T_{min}$ .

If time  $t_2$  is shorter than  $T_{min}$ , the SVM signal with the smallest duty cycle is shifted to the right to ensure enough time for current measurement during vector  $\vec{V}_2$ , as shown in Figure 8a. In case  $t_1$  is shorter than  $T_{min}$ , the SVM signal with the largest duty cycle is shifted to the left to ensure enough time for current measurement during vector  $\vec{V}_1$ , as shown in Figure 8b.

The proposed SVM modification method does not solve a problem with an unreachable area and boundary area 2. Inside an unreachable area, the SVM duty cycle is large and similar for all three phases. Inside the boundary area 2, the SVM duty cycle is short and similar for all three phases. The SVM shift approach is not useful inside an unreachable area and boundary area 2, since the SVM signal cannot be shifted with values lower than 0% and higher than 100%. Using similar SVM patterns, shown in Section 2 for Regions 2, 3, and 4, a problem with an unreachable area can be solved. Boundary area 2 inside Region 1 is not covered with this method.

Figure 9b shows the proposed SVM pattern modification that allows us to generate an arbitrary voltage vector inside an unreachable area using the same vector combination as used for Region 2. Table 6 shows the formulas used for the proposed SVM pattern modification shown in Figure 9b.



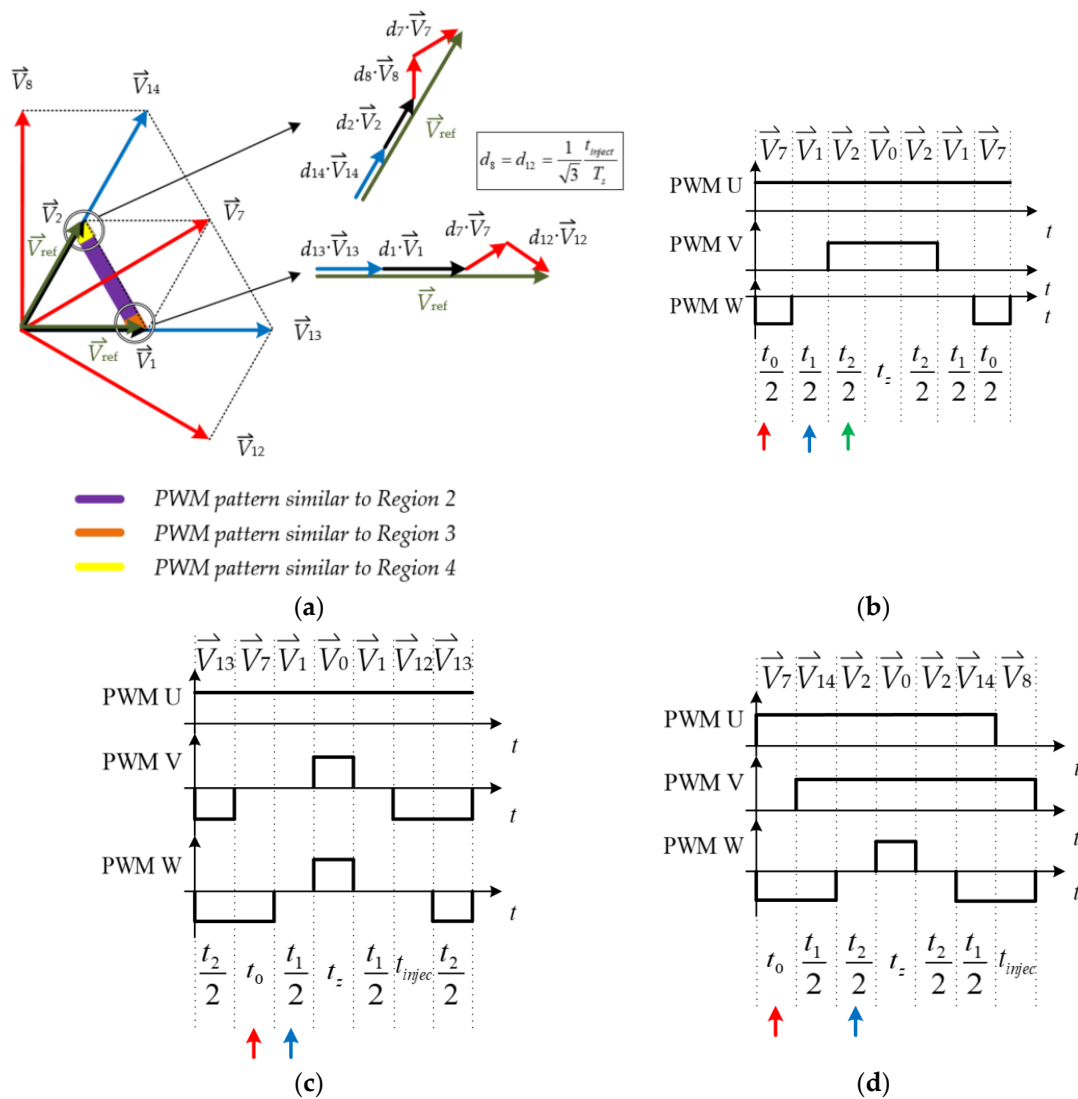


**Figure 9.** (a) Vector limitation using the proposed modified SVM pattern for the central part of an unreachable area; (b) proposed modified SVM pattern used for the central part of an unreachable area; (c) proposed modified SVM pattern used for an unreachable area close to Region 3; (d) proposed modified SVM pattern used for an unreachable area close to Region 4.

**Table 6.** Time calculation for the proposed SVM pattern for Region 2 applied inside the inner hexagon.

Parameter	Formula
$t_0$	$1.5 \cdot T_{\min}$
$t_2$	$\frac{6}{\sqrt{3}} \frac{U_{ref,y}}{U_{DC}} T_s - t_0$
$t_1$	$3 \cdot \frac{U_{ref,x}}{U_{DC}} T_s - \frac{1}{2} t_2 - \frac{3}{2} t_0$
$t_z$	$T_s - t_1 - t_2 - t_0$

Setting time  $t_0$  to a fixed value that is longer than  $T_{\min}$  allows us to measure current during vector  $\vec{V}_7$  the whole time. If  $t_1$  is longer than  $t_2$ , a second current measurement is done during vector  $\vec{V}_1$ , otherwise the current measurement is done during vector  $\vec{V}_2$ . Setting time  $t_0$  to a fixed value has a negative side effect, which is limiting the minimum and maximum reachable arbitrary voltage vector angles. In other words, the proposed SVM pattern and usage of the same vector combination as for Region 2 does not solve the problem with the whole unreachable area inside Region 1.

Figure 9a shows the area that still cannot be reached despite the proposed SVM pattern shown in Figure 9b. Such areas are marked with yellow and orange colors. The proposed SVM patterns shown in Figure 9c,d can be used to cover these areas as well. The orange area can be covered with the SVM pattern shown in Figure 9c, and the yellow area can be covered with the SVM pattern shown in Figure 9d. The linear vector combinations used to cover the orange and yellow areas are also presented in Figure 9a, where injected vectors can be seen. The expressions of the proposed SVM pattern modification in Figure 9c are presented in Table 7. Table 8 shows the formulas used for the proposed SVM pattern modification shown in Figure 9d.

**Table 7.** Time calculation for the proposed SVM pattern for Region 3 applied inside the inner hexagon.

Parameter	Formula
$t_0$	$1.5 \cdot T_{\min}$
$t_1$	$3 \cdot T_{\min}$
$t_{injec}$	$t_0 - \frac{6}{\sqrt{3}} \frac{U_{ref,y}}{U_{DC}} T_s$
$t_2$	$\frac{3}{2} \cdot \frac{U_{ref,x}}{U_{DC}} \cdot T_s - \frac{1}{2} t_1 - \frac{3}{4} \cdot (t_0 + t_{injec})$
$t_z$	$T_s - t_1 - t_2 - t_0 - t_{injec}$

**Table 8.** Time calculation for the proposed SVM pattern for Region 4 applied inside the inner hexagon.

Parameter	Formula
$t_0$	$1.5 \cdot T_{\min}$
$t_2$	$3 \cdot T_{\min}$
$t_1$	$3 \cdot \frac{U_{ref,x}}{U_{DC}} \cdot T_s - \frac{1}{2} t_2 - \frac{3}{2} \cdot t_0$
$t_{injec}$	$t_{injec} = \sqrt{3} \frac{U_{ref,y}}{U_{DC}} T_s - \frac{1}{2} (t_2 + t_0) - t_1$
$t_z$	$t_z = T_s - t_1 - t_2 - t_0 - t_{injec}$

### 3.2. SVM Pattern Modification Inside Region 2

Figure 10a shows Region 2 inside Sector 1, divided into a few areas in an equivalent way as described for Region 1. With the linear combination of basic voltage vectors  $\vec{V}_1$ ,  $\vec{V}_2$ , and  $\vec{V}_7$ , an arbitrary voltage vector is obtained, as also shown in Figure 10a. The SVM pattern for the normal operating area inside Region 2 is shown in Figure 10b.

Region 2 differs from other regions, since all three-phase currents can be measured within a switching period, which gives us more flexibility for current measurement.

Figure 10c shows the case in which the arbitrary voltage vector is positioned inside the boundary area 1, close to Region 3. In such a case, time  $t_2$  is shorter than  $T_{\min}$ . The current can still be measured twice within a switching period, during vectors  $\vec{V}_1$  and  $\vec{V}_7$ , even when time  $t_2$  is shorter than  $T_{\min}$ . Figure 10d shows the case in which the arbitrary voltage vector is positioned inside the boundary area 1, close to Region 4. In such a case, time  $t_1$  is shorter than  $T_{\min}$ .

In addition, the current can be measured twice within a switching period during vectors  $\vec{V}_7$  and  $\vec{V}_2$ . Figure 10e shows the case in which the arbitrary voltage vector is positioned inside the boundary area 1, close to Region 1. In such a case, time  $t_0$  is shorter than  $T_{\min}$ . The current also can be measured twice within a switching period, during vectors  $\vec{V}_1$  and  $\vec{V}_2$ . Based on the time window between the SVM edges, the current sampling position can simply be changed to a position where current measurement is possible, and with such an approach, SVM modification can be avoided.

Such an approach is not possible in some parts of the boundary area. These parts are marked with the orange area in Figure 10a. In such areas, only one current measurement is possible. The previously described method for Region 1 can be used to solve a problem within the orange area.

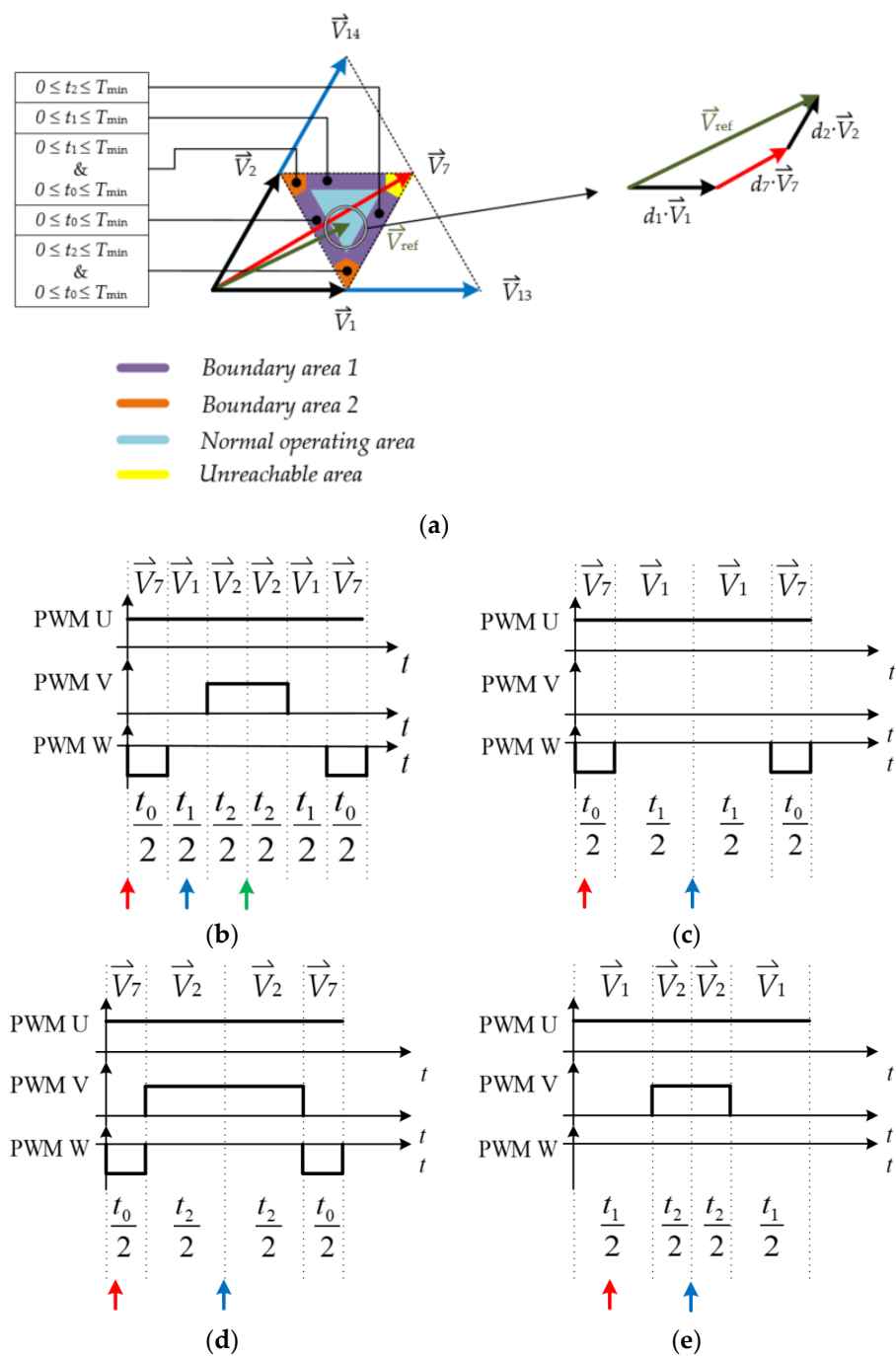


**Figure 10.** (a) Vector diagram for Sector 1 and Region 2 with marked problematic areas for single-shunt measurement; (b) SVM pattern for Sector 1 and Region 2 inside the normal operating area; (c) SVM pattern while  $t_2 = 0$  s; (d) SVM pattern while  $t_1 = 0$  s; (e) SVM pattern while  $t_0 = 0$  s.

### 3.3. SVM Pattern Modification Inside Region 3

Figure 11a shows Region 3 inside Sector 1, divided into areas like those described for Regions 1 and 2. With the linear combination of basic voltage vectors  $\vec{V}_1$ ,  $\vec{V}_7$ , and  $\vec{V}_{13}$ , an arbitrary voltage vector is obtained, as also shown in Figure 11a. The SVM pattern for the normal operating area inside Region 3 is shown in Figure 11b. Figure 11c shows the case in which the arbitrary voltage vector is aligned with the basic voltage vectors  $\vec{V}_1$  and  $\vec{V}_{13}$ . Since current does not flow through the shunt during vector  $\vec{V}_{13}$ , current measurement is possible only during vector  $\vec{V}_1$ , which is not enough for current reconstruction. Figure 11d

shows the case where the arbitrary voltage vector is positioned inside the boundary area 1, close to Region 2. In such a case, time duration  $t_2$  is shorter than  $T_{min}$ . The current through the shunt can be measured twice within a switching period during vectors  $\vec{V}_7$  and  $\vec{V}_1$ .

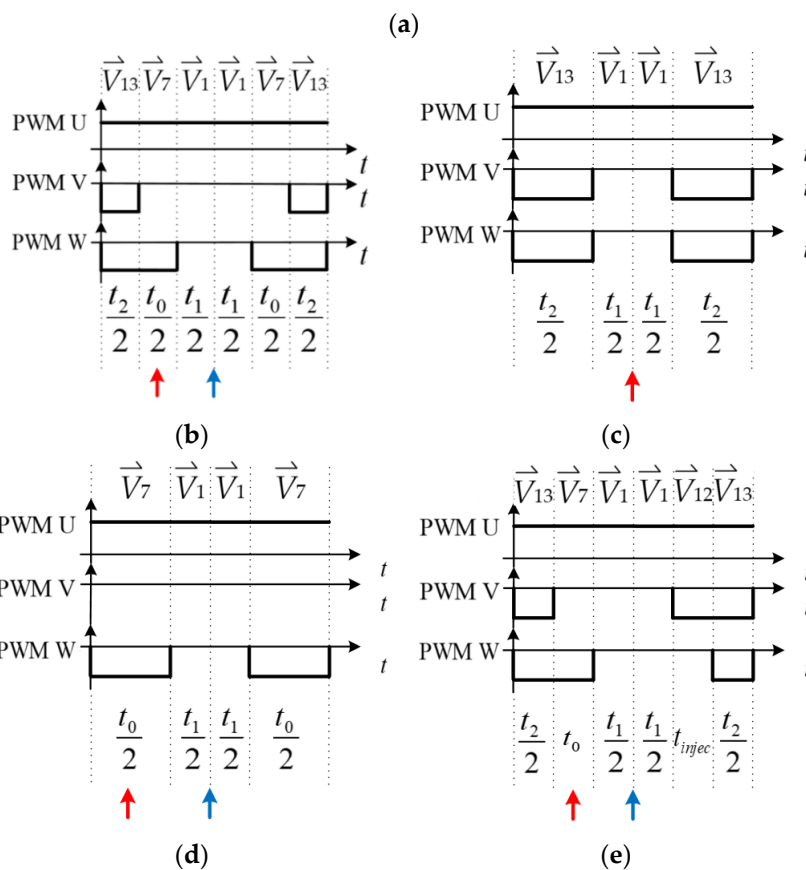
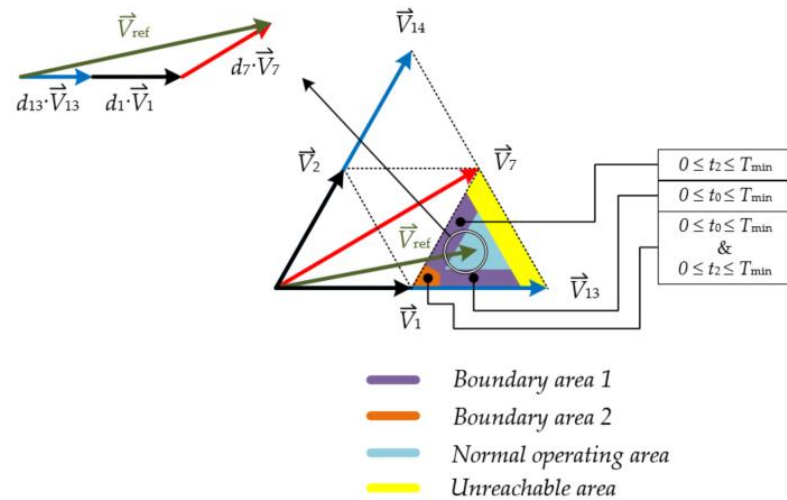


**Figure 11.** (a) Vector diagram for Sector 1 and Region 3 with marked problematic areas for single-shunt measurement; (b) SVM pattern for Sector 1 and Region 3 inside the normal operating area; (c) SVM pattern while  $t_0 = 0$  s; (d) SVM pattern while  $t_2 = 0$  s; (e) proposed SVM modification pattern while  $t_0 < T_{min}$ .

As can be seen, the problem inside Region 3 occurs while the arbitrary voltage vector is aligned or close to vectors  $\vec{V}_1$  and  $\vec{V}_{13}$ . The SVM-shift approach, like that described for Region 1, can be used, which will cause injection of the new basic voltage vector. Figure 11e shows the SVM shifting approach for Region 3. The idea is to shift the SVM signals in such

a way that the arbitrary voltage vector stays unchanged, and at the same time, enough time shall be ensured for current measurement. This is possible when two SVM signals are shifted at the same time: The SVM signal for phase W needs to be shifted to the right, and the SVM signal for phase V needs to be shifted to the left. SVM shifting causes injection of vector  $\vec{V}_{12}$  like that shown in Figure 11e. The equations used for time calculation are shown in Table 9.

**Table 9.** Time calculation for the proposed SVM pattern for Region 3 applied inside the outer hexagon.

Parameter	Formula
$t_0$	$1.5 \cdot T_{\min}$
$t_{injec}$	$t_0 - 2\sqrt{3} \cdot \frac{U_{ref,y}}{U_{DC}} \cdot T_s$
$t_2$	$3 \frac{U_{ref,x}}{U_{DC}} T_s - T_s - \frac{1}{2} \cdot (t_0 + t_{injec})$
$t_1$	$2 \cdot T_s - \frac{1}{2} (t_0 + t_{injec}) - 3 \frac{U_{ref,x}}{U_{DC}} T_s$

When the arbitrary voltage vector is positioned close to Regions 2 and 3, which is shown with the orange area inside Figure 11a, the previously proposed SVM-shift method cannot be used, since time durations  $t_0$  and  $t_2$  are shorter than  $T_{\min}$ . In such a case, the SVM pattern described for Region 1 is used, shown in Figure 9c. Using the proposed SVM-shift method for Region 3, the unreachable area could not be reached, which will reduce the maximum available modulation index.

### 3.4. SVM Pattern Modification Inside Region 4

Figure 12a shows Region 4 inside Sector 1 divided into areas like those described for Regions 1–3. With the linear combination of basic voltage vectors  $\vec{V}_2$ ,  $\vec{V}_7$ , and  $\vec{V}_{14}$ , an arbitrary voltage vector is obtained, as also shown in Figure 12a. The SVM pattern for the normal operating area inside Region 4 is shown in Figure 12b. Figure 12c shows the case in which the arbitrary voltage vector is positioned inside the boundary area 1, close to Region 2. In such a case, time duration  $t_1$  is shorter than  $T_{\min}$ . The current can be measured twice within a switching period, during vectors  $\vec{V}_7$  and  $\vec{V}_2$ . The case in which the arbitrary voltage vector is aligned with the basic voltage vectors  $\vec{V}_2$  and  $\vec{V}_{14}$  is shown in Figure 12d. Since current does not flow through the shunt during vector  $\vec{V}_{14}$ , current measurement is possible only during vector  $\vec{V}_2$ , which is not enough for current reconstruction.

The problem inside Region 4 occurs while the arbitrary voltage vector is aligned or close to vectors  $\vec{V}_2$  and  $\vec{V}_{14}$ . A similar SVM shift approach like that described for Region 3 is used and shown in Figure 12e.

The SVM signal for phase V needs to be shifted to the left, and the SVM signal for phase U needs to be shifted to the right. SVM shifting causes injection of vector  $\vec{V}_8$ , as shown in Figure 12e. The equations used for the time calculation are shown in Table 10.

**Table 10.** Time calculation for the proposed SVM pattern for Region 4 applied inside the outer hexagon.

Parameter	Formula
$t_0$	$1.5 \cdot T_{\min}$
$t_{injec}$	$\frac{\sqrt{3}U_{ref,y} - 3U_{ref,x}}{U_{DC}} T_s + t_0$
$t_1$	$\frac{\sqrt{3}U_{ref,y} + 3U_{ref,x}}{U_{DC}} T_s - t_0 - T_s$
$t_2$	$2T_s - t_0 - 2\sqrt{3} \frac{U_{ref,y}}{U_{DC}} T_s$

If the arbitrary voltage vector is positioned close to Regions 2 and 4, which is shown with an orange area inside Figure 12a, the previously proposed SVM-shift method cannot be used, since time durations  $t_0$  and  $t_1$  are smaller than  $T_{\min}$ . In such a case, the SVM

pattern described for Region 1 is used, as shown in Figure 9d. Using the proposed SVM shift method for Region 4, the unreachable area could not be reached, which will reduce the maximum available modulation index.

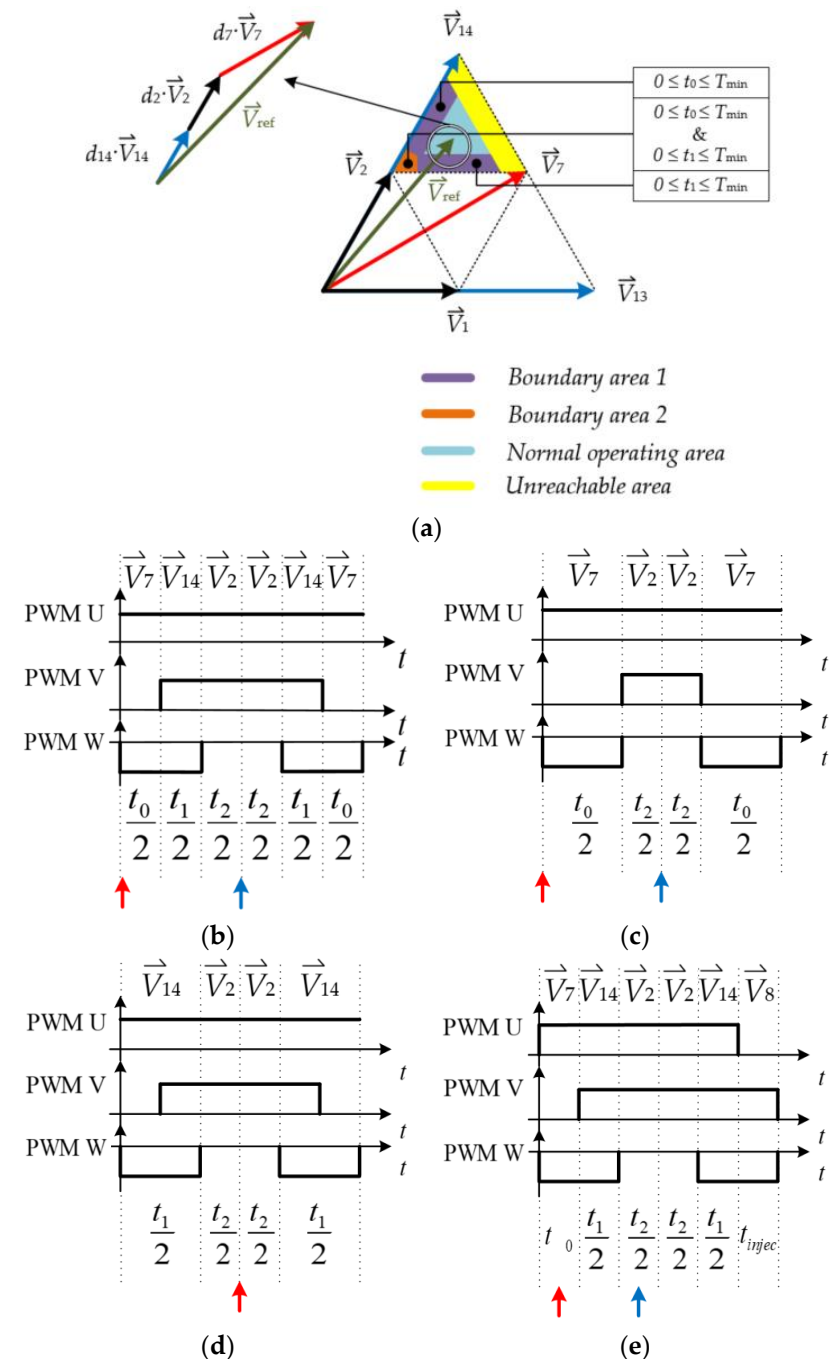


**Figure 12.** (a) Vector diagram for Sector 1 and Region 4 with marked problematic areas for single-shunt measurement; (b) SVM pattern for Sector 1 and Region 4 inside the normal operating area; (c) SVM pattern while  $t_1 = 0$  s; (d) SVM pattern while  $t_0 = 0$  s; (e) proposed SVM modification pattern while  $t_0 < T_{min}$ .

#### 4. Hardware Implementation

A digital signal processor is used for SVM signal generation, ADC current measurement, space-vector modulator calculation, single-shunt current-measurement reconstruction, and communication with a PC. Figure 13 shows a block scheme of all the proposed



tasks for control of the three-level inverter. The voltage reference vector length and frequency are obtained through serial communication from the PC.

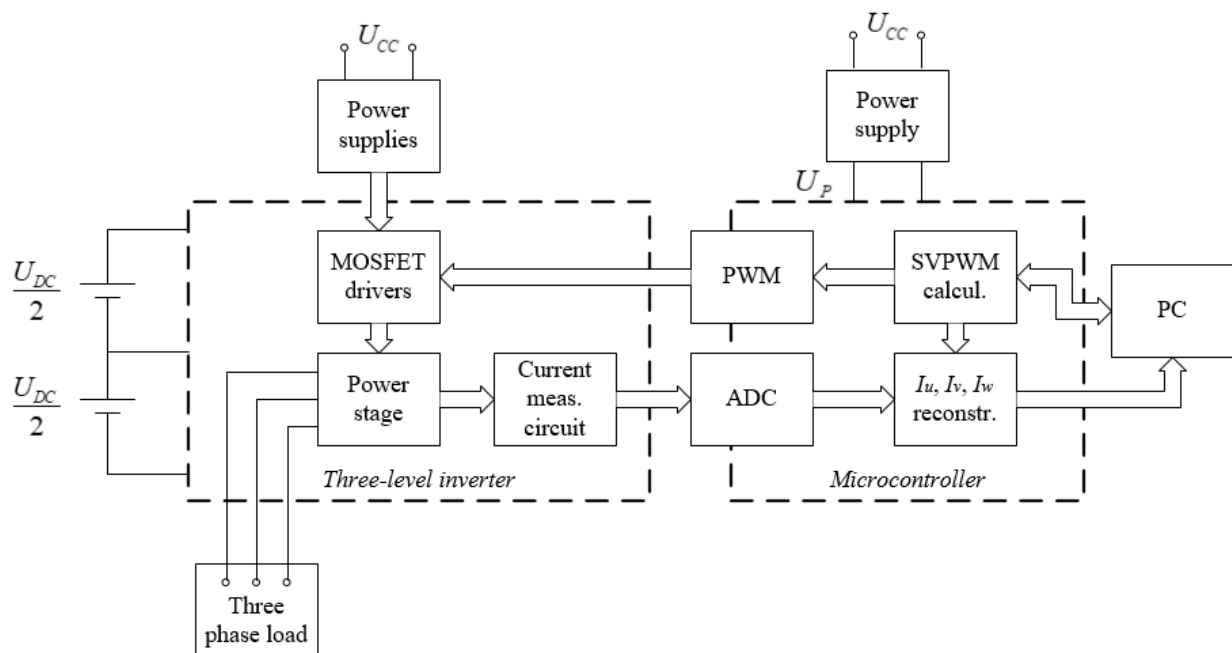


**Figure 13.** The block scheme of a three-level inverter.

After calculation of the space-vector modulation, the SVM signals are set and voltage is applied to the load. Based on the calculated space-vector-modulation parameters, two current measurements are taken using the current-measurement circuit and the current reconstruction is then executed, and the results are sent to the PC. Results are shown graphically in a runtime using the software X2C Scope.

#### 4.1. Electronic Circuits

The three-level inverter was designed for a power range up to 100 W. It is switched with the frequency of 16 kHz. The shunt resistor and current measurement circuit ensure a current-measurement range up to 16 A, with the minimum settling time window equal to 3.2  $\mu$ s. The three-level inverter is loaded with a symmetric  $RL$  load ( $L_U = L_V = L_W = 560 \mu\text{H}$ ,  $R_U = R_V = R_W = 5.1 \Omega$ ). Based on the proposed block diagram in Figure 12, the power stage was designed and built as shown in Figure 13.

##### 4.1.1. Power Stage Circuit

The three-level inverter was supplied from two 12 V power supplies connected to DC link capacitors. The power stage consisted of four MOSFETs (IPB120N08S4-03) and two bypass diodes (V30DM120HM3) per phase as a basic part of a three-level inverter, and dual isolated gate drivers were used for MOSFET driving. The shunt resistor was connected to the neutral point of the three-level inverter ( $R_{Sh} = 5 \text{ m}\Omega$ ) for current measurement.

##### 4.1.2. Current-Measurement Circuit

One of the crucial parts dealing with single-shunt measurement is the current-measurement circuit. With the quality of current-measurement circuit design, utilization of the DC link voltage can be influenced by reducing the minimum settling time  $T_{\min}$  needed for measurement. Figure 14 shows the implemented current-measurement circuit. The current-measurement circuit must fulfill the following requirements:

- The output signal is a DC signal with maximum range up to 3 V.

- The current-measurement range is 20% greater than the maximum expected, to ensure current measurement for the whole current range with enough assurance.
- The bandwidth is greater than 1 MHz.

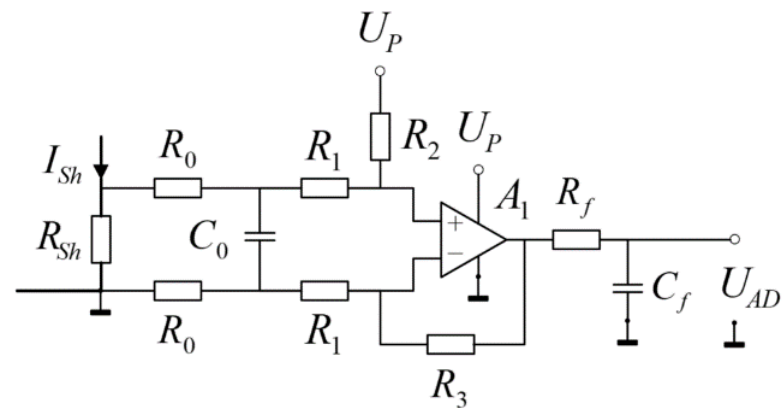


Figure 14. Current-measurement circuit.

The current-measurement circuit used is a differential amplifier. The DC offset for the current-measurement circuit shown in Figure 14 is determined with the following expression:

$$U_{offset} = \frac{R_0 + R_1}{R_0 + R_1 + R_2} \left( 1 + \frac{R_3}{R_0 + R_1} \right) \cdot U_P \quad (5)$$

and the operational amplifier gain can be calculated as follows:

$$A_V = \left( 1 + \frac{R_2}{R_0 + R_1} \right) \quad (6)$$

The operational amplifier DC offset was set to 1.7 V, and the gain to 16.69 ( $R_0 = R_1 = 510 \Omega$ ,  $R_2 = 32 \text{ k}\Omega$ ,  $R_3 = 16 \text{ k}\Omega$ ,  $U_p = 3.3 \text{ V}$ ). The selected operational amplifier (OPA365AIDBVR) had a gain bandwidth of 50 MHz, which gave us a bandwidth for current measurement greater than 1 MHz. The output filter time constant was set to 10 ns ( $R_f = 100 \Omega$ ,  $C_f = 100 \text{ pF}$ ).

#### 4.1.3. Digital Signal Processor

A control board (F28335 control card, Texas Instruments) with a digital signal processor (TMS320F28335ZJZA) was used for three-level inverter control. The DSP was equipped with:

- High-performance 32-bit CPU (TMS320C28x);
- 12-bit Analog–digital converter (ADC);
- Six-channel DMA controller (for ADC, ePWM, etc.);
- Up to 18 PWM outputs;
- Serial port peripherals, etc.

Figure 15 shows the docking station with control board and DSP.

The DSP unit can achieve ADC measurement with an 80 ns conversion rate. The control board with docking station is capable of communicating with the PC through serial communication. The key features of this module are fast ADC conversion, a high enough number of SVM channels, flexible ADC triggering, and the possibility to achieve different communication protocols very easily.

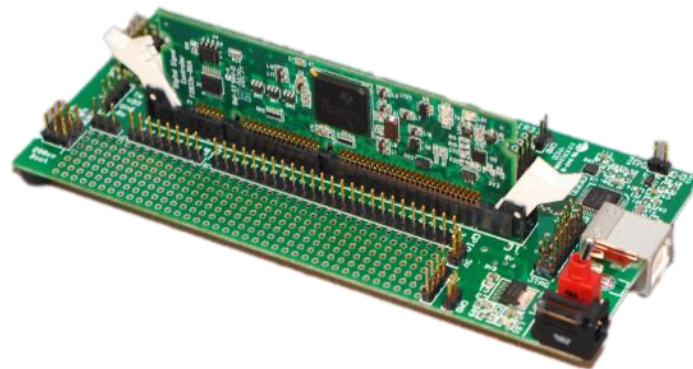


**Figure 15.** Docking station with control board and DSP.

#### 4.1.4. Power Supplies

DC–DC power supplies with galvanic isolation were used for safety reasons. MOSFET drivers were supplied with a double-output 12 V isolated power supply (R1DA-121212/P, RECOM Power). The docking station with control board and DSP was supplied with external 5 V (TES 5-1212, TRACO Power). The docking station was equipped with a voltage regulator that supplied the DSP with 3.3 V.

### 5. Experimental Results

The described single-shunt current-measurement algorithm was verified using the test-bench system shown in Figure 16. The current through the shunt was measured twice inside the switching period, as described in Sections 2 and 3, using DSP. Then, the DSP reconstructed the phase currents and forwarded the results to the PC through serial communication. Using an X2C Scope, results were shown graphically in runtime.

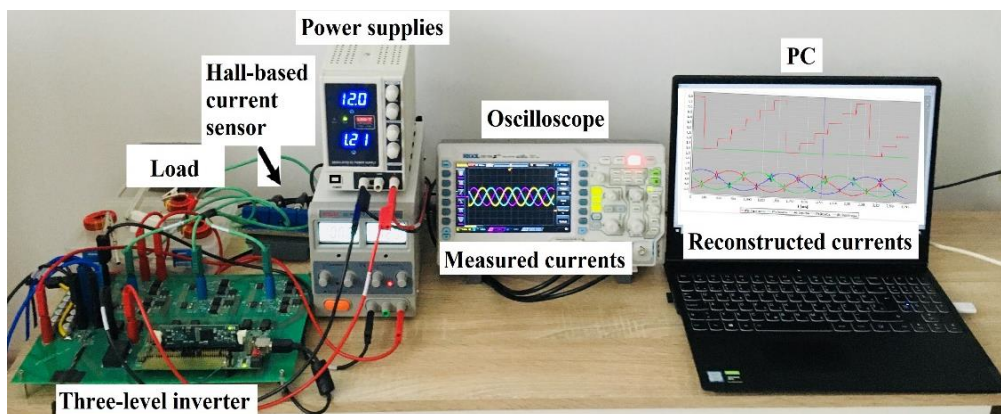


**Figure 16.** Measurement test-bench used for verification of the proposed SVM algorithm.

#### 5.1. Experimental Test-Bench

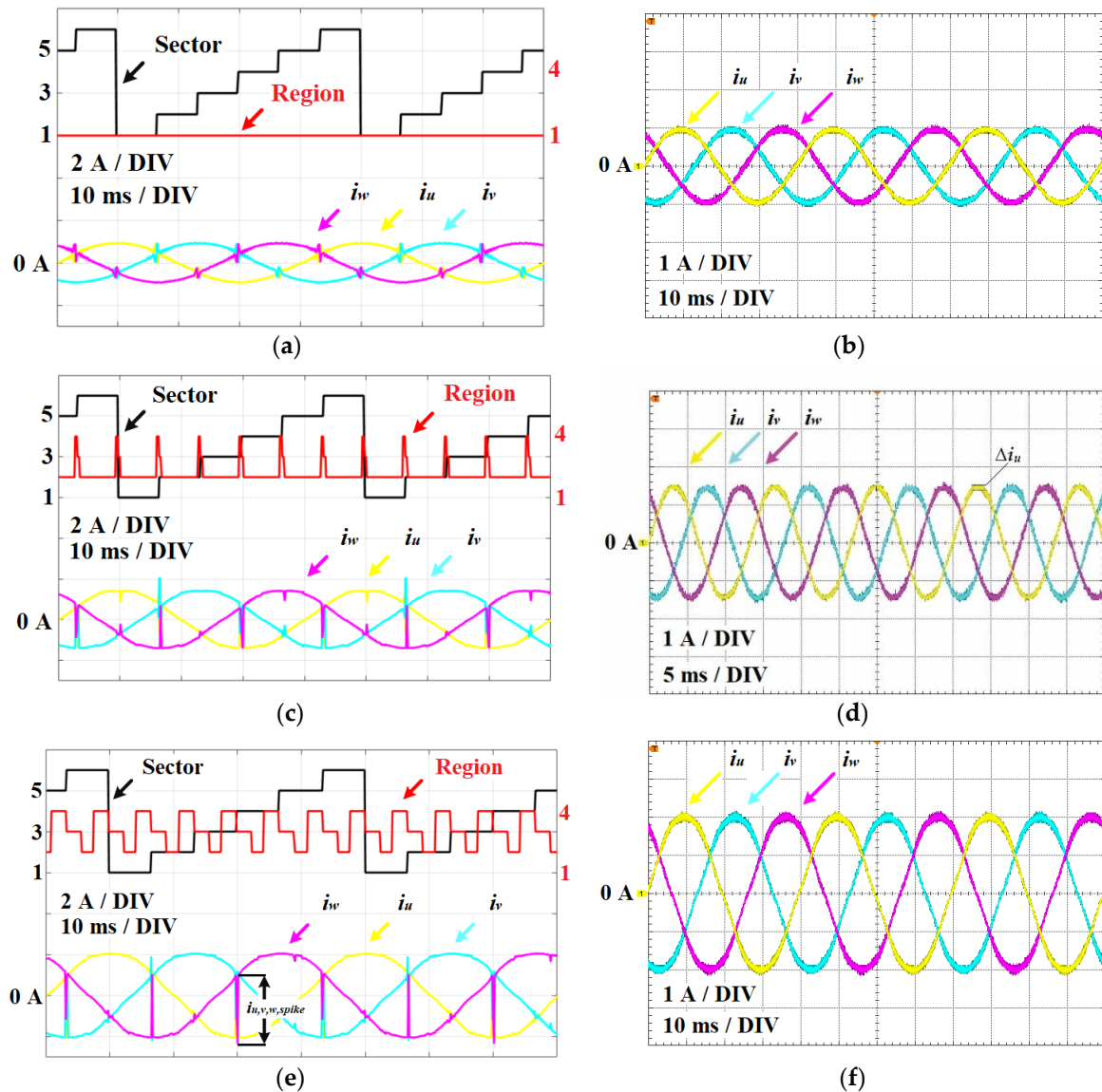
The proposed algorithm was verified using the test-bench system shown in Figure 16. For verification purposes, the phase currents were measured using oscilloscope measurement (as a reference system), and compared to the reconstructed currents obtained through the serial communication, as described in Section 4. Measurements for the proposed algorithms with and without modification were performed at the same operating points.

#### 5.2. Measurement Results

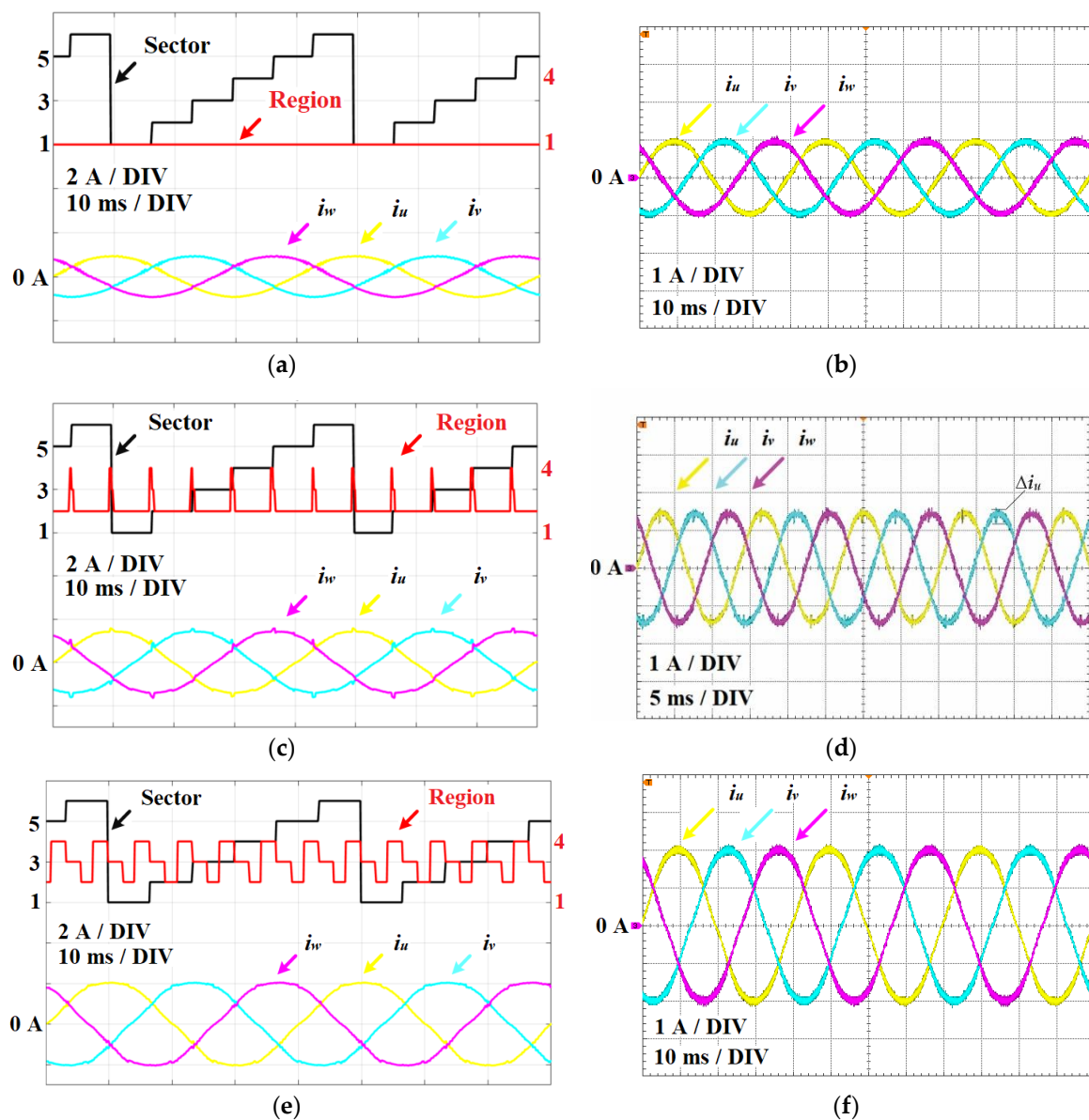
The designed three-level inverter was tested under laboratory conditions. To verify the single-shunt current-reconstructions' measurement results, these were compared with the reference currents measured with the oscilloscope. Measurements were done for different values of modulation index as a function of the load frequency (at 25, 50, and 75 Hz). Test

cases were chosen to cover the critical cases in the vicinity of the sector and region of vector's boundaries as described in previous sections.

The results obtained when ordinary space-vector modulation (SVM) was used showed the expected current spikes close to the sector and region boundaries. Figures 17 and 18 show the current-reconstruction results and current measured by current sensors on the scope. Figure 17a–f show the measurement results when the load frequency of 25 Hz was applied. The maximum absolute current spike appeared when the modulation index was designated to  $m_i = 0.6$  (Figure 17e) and it was measured at  $i_{u,v,w,spike} = 3.4$  A.



**Figure 17.** Single-shunt reconstruction of a three-phase current without SVM modification for  $f = 25$  Hz: (a)  $m_i = 0.4$ ; (c)  $m_i = 0.6$ ; (e)  $m_i = 0.8$ ; scope-measured real three-phase currents for  $f = 25$  Hz: (b)  $m_i = 0.4$ ; (d)  $m_i = 0.6$ ; (f)  $m_i = 0.8$ .



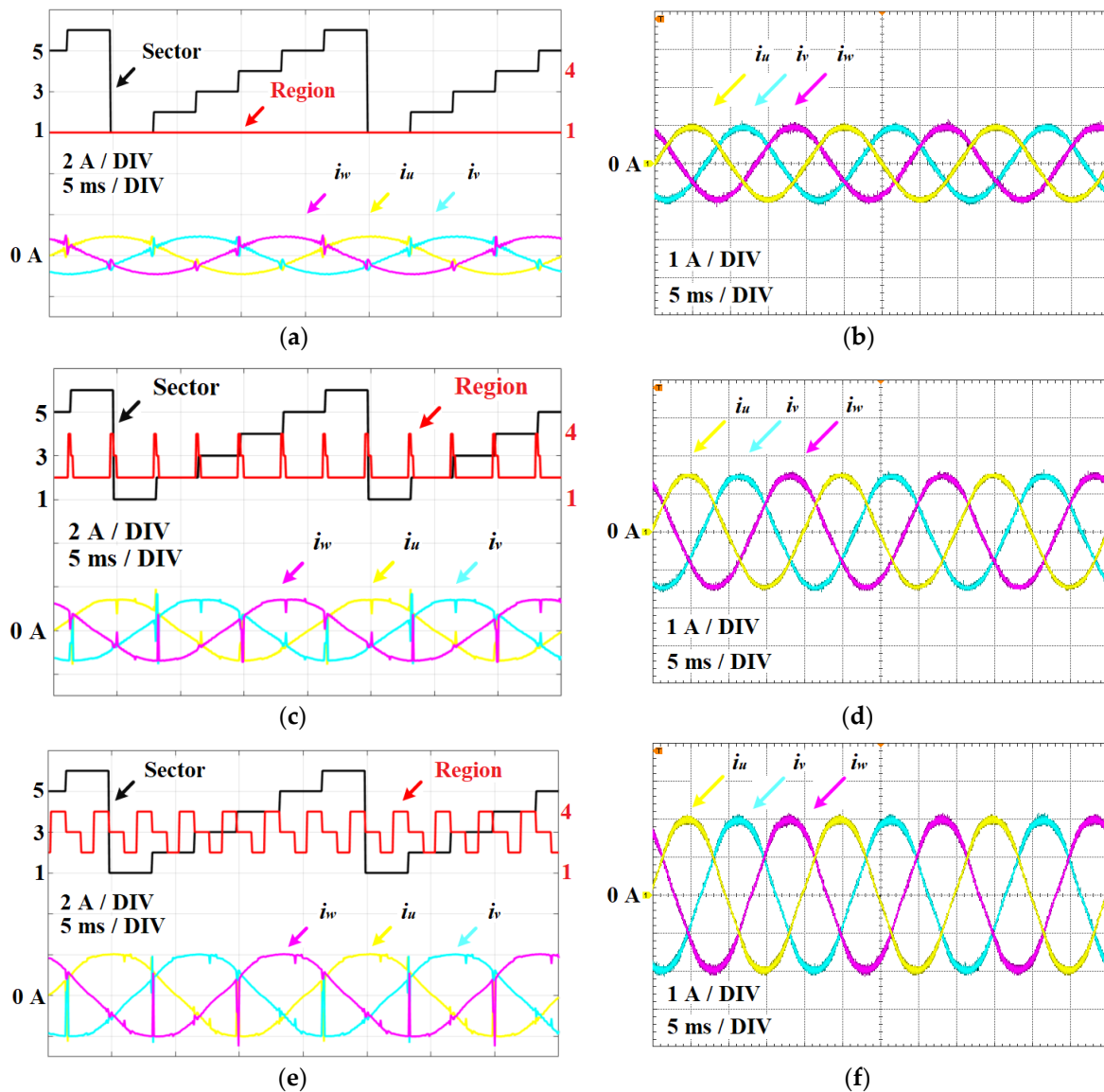
**Figure 18.** Single-shunt reconstruction of a three-phase current with SVM modification for  $f = 25$  Hz: (a)  $m_i = 0.4$ ; (c)  $m_i = 0.6$ ; (e)  $m_i = 0.8$ ; scope-measured real three-phase currents for  $f = 25$  Hz: (b)  $m_i = 0.4$ ; (d)  $m_i = 0.6$ ; (f)  $m_i = 0.8$ .

Figure 18a–f show the measured results when modified SVM was applied (Section 3). In this case, the current reconstruction was also feasible in the boundary region using the single-shunt current-measurement signal, as was described in the previous sections. The current spikes almost disappeared, as can be seen in Figure 18c, and the signal was measured at  $i_{u,v,w,spike} = 0.17$  A. In addition, as was mentioned previously, the modified SVM caused an increase in the load current ripple. In the case of ordinary SVM, the current ripple was measured at  $\Delta i_u = 0.16$  A peak-to-peak (pp) (Figure 17d), when the modulation index was set to  $m_i = 0.6$  (worst case). Due to the vector injection in the case of modified SVM, the current ripple increased to  $\Delta i_u = 0.16$  A peak-to-peak (pp) (Figure 18d). Rather than comparison of the absolute values of the current ripple, which was also dependent of the load inductance, it can be concluded that modified SVM caused the double current ripple in the vicinity of the sector and region boundaries when modified SVM was applied.

Figures 19 and 20 show the current reconstruction when the load frequency of 50 Hz was required. The results when ordinary SVM was applied are shown in Figure 19a–f, and when modified SVM was applied, are presented in Figure 20a–f. In a similar way to a load frequency of 25 Hz, the results obtained for a load frequency of 50 Hz also had



an expected current spike close to the sector and region boundaries, with the measured maximum absolute current spike at  $i_{u,v,w,spike} = 3.4$  A (Figure 19e); and when modified SVM was used, the current spike was practically unmeasurable ( $i_{u,v,w,spike} = 0.18$  A, Figure 20e). These performance parameters are indicated in Table 11.



**Figure 19.** Single-shunt reconstruction of a three-phase current without SVM modification for  $f = 50$  Hz: (a)  $m_i = 0.4$ ; (c)  $m_i = 0.6$ ; (e)  $m_i = 0.8$ ; scope-measured real three-phase currents for  $f = 50$  Hz: (b)  $m_i = 0.4$ ; (d)  $m_i = 0.6$ ; (f)  $m_i = 0.8$ .



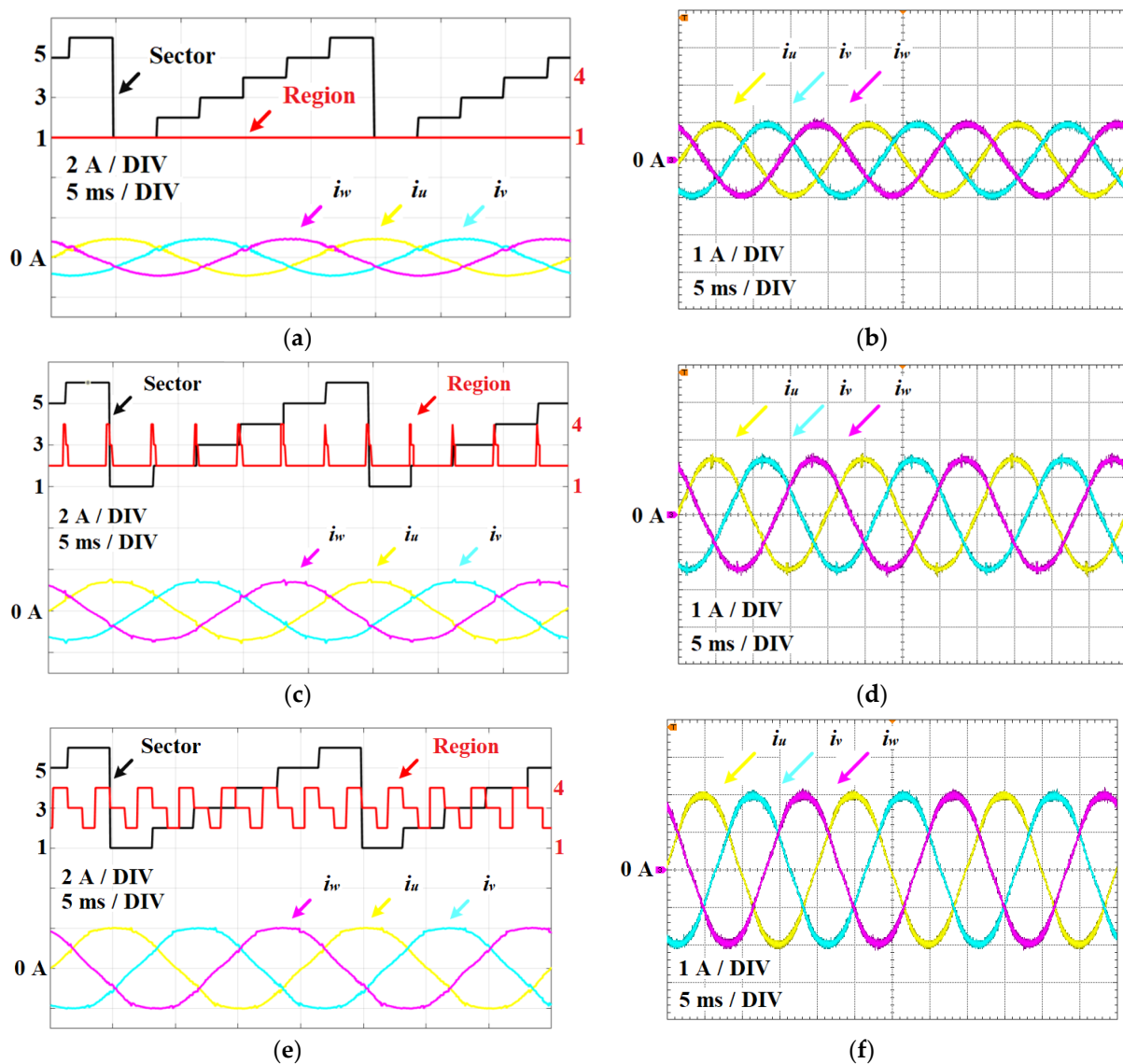


**Figure 20.** Single-shunt reconstruction of a three-phase current with SVM modification for  $f = 50$  Hz: (a)  $m_i = 0.4$ ; (c)  $m_i = 0.6$ ; (e)  $m_i = 0.8$ ; scope-measured real three-phase currents for  $f = 50$  Hz: (b)  $m_i = 0.4$ ; (d)  $m_i = 0.6$ ; (f)  $m_i = 0.8$ .

Figures 21 and 22 show the results of current reconstruction when the load frequency of 75 Hz was applied. Figure 21a–f show the three-phase currents' reconstruction results when the ordinary SVM was used (Section 2). The modulation index was chosen so that the current reconstruction is visible on the boundary areas of the sectors and regions. The current spike was measured at  $i_{u,v,w,spike} = 3.15$  A (Figure 21e). Figure 22a–f show the results obtained when the modified SVM algorithm was applied as described in Section 3. The current spike was negligible, and it was measured at  $i_{u,v,w,spike} = 0.15$  A (Figure 22e).

Table 11. Performance index for measurement results.

Frequency [Hz]	Modulation Index $m_i$	Measurement without SVM Modification	Measurement with SVM Modification	Scope Measurement $I_{f-rms}$ [A]	Maximum Absolute Peak-Current Error $I_{f-peak,error}$ [A]	Relative Error $\epsilon$ [%]
		$I_{f-rms,SVM,non-modified}$ [A]	$I_{f-rms,SVM,modified}$ [A]			
25	0.4	0.662	0.655	0.689	0.52	4.93
	0.6	1.012	1.020	1.070	2.09	4.67
	0.8	1.472	1.470	1.450	3.40	1.38
50	0.4	0.658	0.652	0.684	0.52	4.68
	0.6	1.007	1.006	1.060	2.17	5.09
	0.8	1.456	1.394	1.430	3.28	2.52
75	0.4	0.647	0.647	0.675	0.52	4.15
	0.6	0.960	0.983	1.040	2.30	5.48
	0.8	1.435	1.407	1.410	3.15	0.21

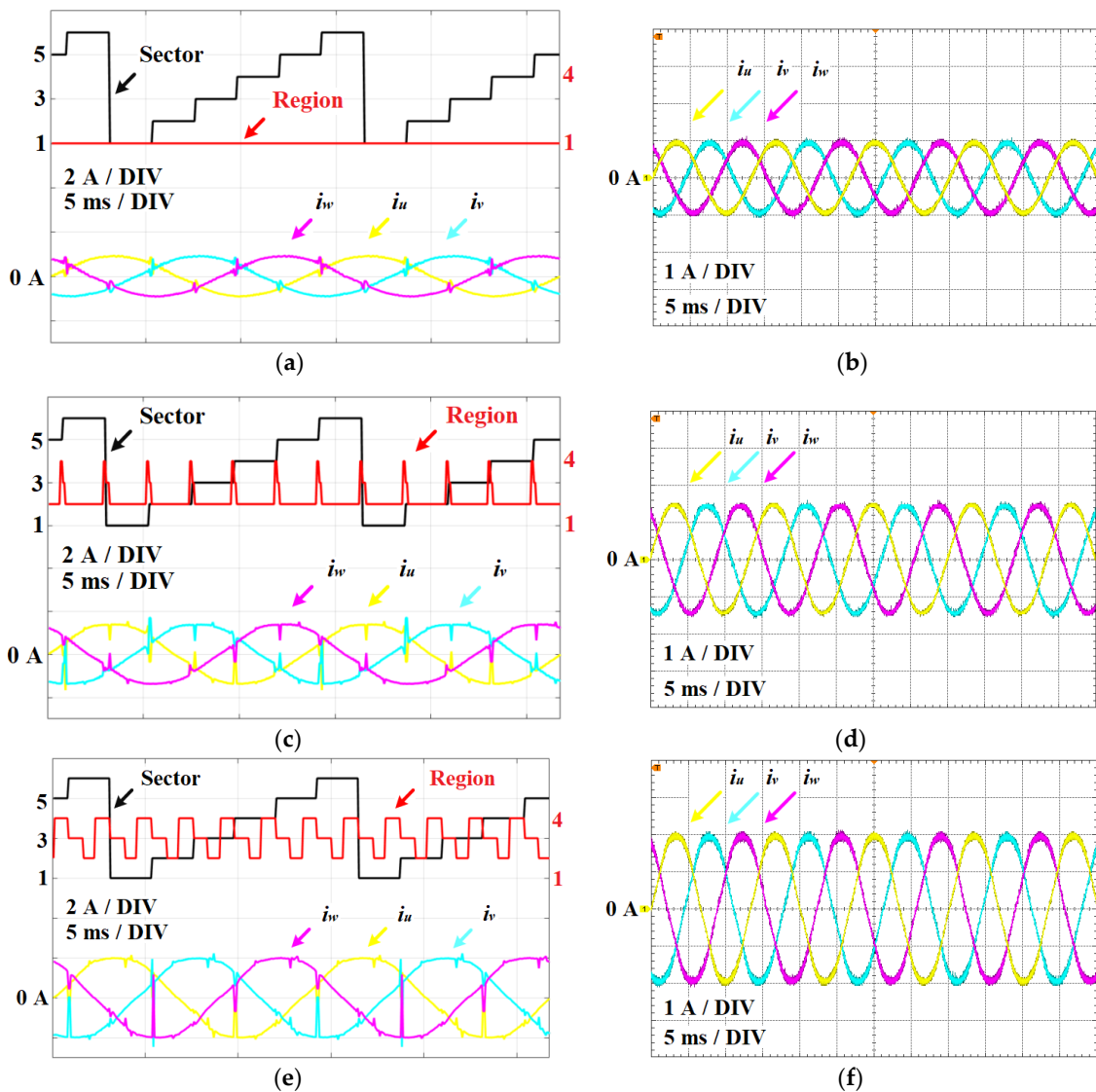
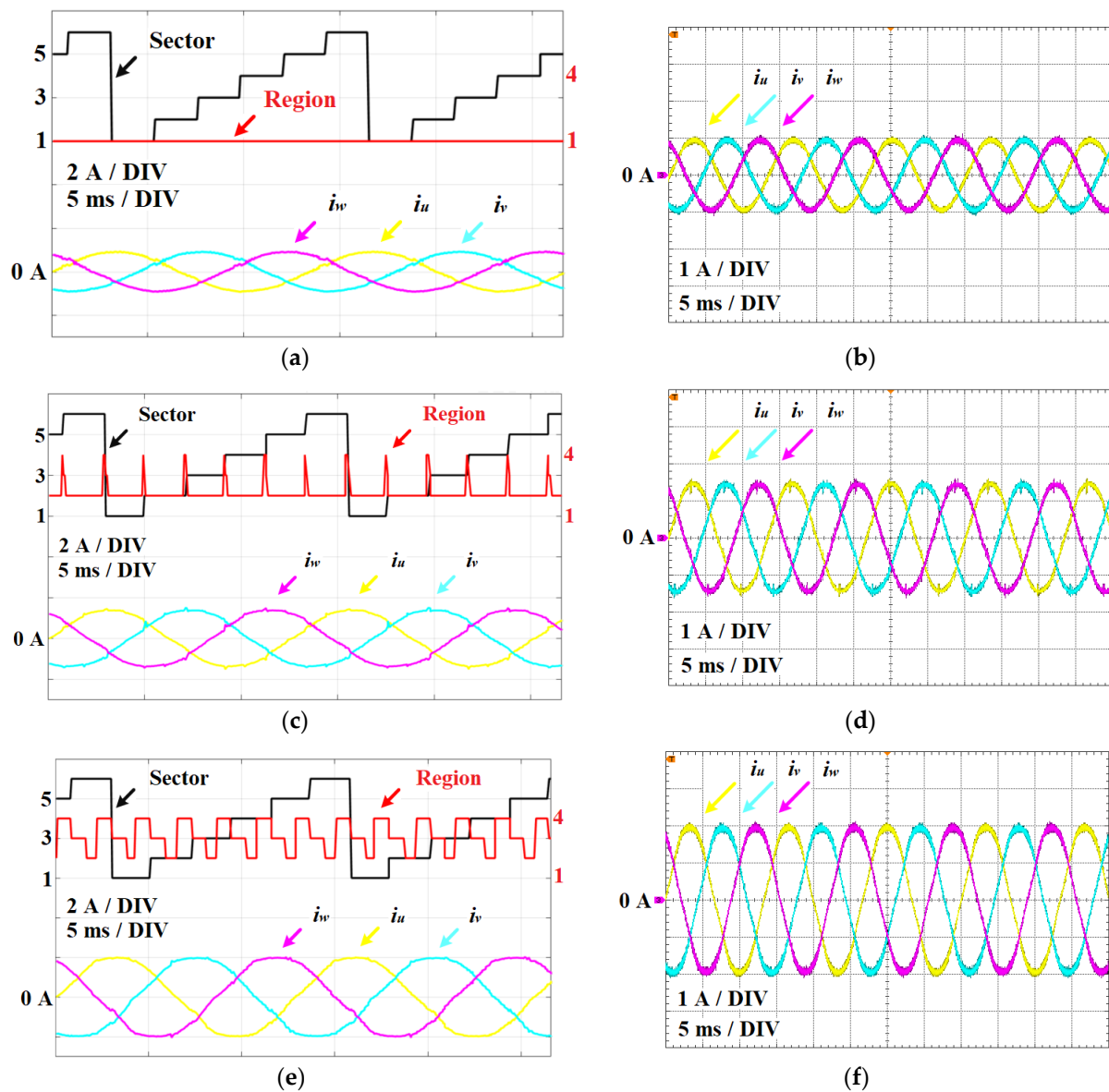


Figure 21. Single-shunt reconstruction of a three-phase current without SVM modification for  $f = 75$  Hz: (a)  $m_i = 0.4$ ; (c)  $m_i = 0.6$ ; (e)  $m_i = 0.8$ ; scope-measured real three-phase currents for  $f = 75$  Hz: (b)  $m_i = 0.4$ ; (d)  $m_i = 0.6$ ; (f)  $m_i = 0.8$ .



**Figure 22.** Single-shunt reconstruction of a three-phase current with SVM modification for  $f = 75$  Hz: (a)  $m_i = 0.4$ ; (c)  $m_i = 0.6$ ; (e)  $m_i = 0.8$ ; scope-measured real three-phase currents for  $f = 75$  Hz: (b)  $m_i = 0.4$ ; (d)  $m_i = 0.6$ ; (f)  $m_i = 0.8$ .

The obtained results (Figures 17–22) showed that the proposed modification algorithm solved the problem with current measurement inside critical areas, and removed current spikes’ occurrence, so the proposed modification algorithm can be used for single-shunt current-reconstructions’ measurement.

The relative error was calculated as follows:

$$\varepsilon = \left| \frac{I_{f-rms} - I_{f-rms,PWM,modified}}{I_{f-rms}} \right| \times 100 \tag{7}$$

where  $I_{f-rms}$  is the phase current measured by the scope, and  $I_{f-rms,PWM,modified}$  represents the single-shunt-measured phase current when the SVM modified algorithm was used.

### 6. Discussion

The method presented here enabled the single-shunt current measurement for reconstructing the three-phase load current using a modified SVM approach. The method reduced vector injection to the minimum, and using the property of Region 2, even avoided

SVM shifting by switching between current-sampling positions, while the vector was still in Region 2. The method used the symmetric SVM patterns to avoid the harmonic distortion. While using vector injection to solve problems close to the boundary between the inner and outer hexagons, the measurement had an effect on the current ripple due to the introduced asymmetry. Since the current was measured in the middle of two SVM edges while using asymmetric SVM patterns, a measurement error was introduced, which can be seen in the measurement results where smaller spikes appeared. This happened because the measured current was not equal to the average current in the sampling period. To decrease the measurement error, exact expressions for the sampling position could be investigated, and reconstructed currents could be improved even further.

## 7. Conclusions

The goal of the presented control method was to develop a measurement system for single-shunt three-phase current reconstruction using SVM for a three-level inverter. Due to the current spikes appearing on the sector and region boundaries, a modified SVM was proposed to extract these. Using the described principle, a three-shunt or three-Hall-sensor measurement circuit for three-level inverters could be replaced with a single-shunt current-measurement circuit without negatively affecting the inverter's performance. The functional laboratory test-bench system of a three-level inverter was designed, and the proposed method was verified for different modulation indices, and also at different load-frequency requirements. The results obtained using the proposed single-shunt measurement method were similar to the real current, comparing the measured and reconstructed current shape and RMS value, with maximum relative error for the RMS phase current around 5%. Smaller current spikes occurred around the boundary area between the inner and outer hexagons on the reconstructed phase currents, with maximum absolute current error up to 0.4 A peak-to-peak caused by measurement inaccuracy due to the vector injection. The proposed modified space-vector modulation was verified for modulation index values from 0.15 to up to 0.92. Current-measurement precision could be improved by adjusting the position when current-measurement samples are taken, which should reduce the maximum absolute current error.

**Author Contributions:** H.K. designed the hardware for the three-level inverter under the guidance of L.K., and also performed all the measurements presented here. The analysis of the electronic circuits and necessary software were designed under the guidance of M.M. All authors have read and agreed to the published version of the manuscript.

**Funding:** This research was funded by the Slovenian Research Agency (ARRS).

**Data Availability Statement:** Data are contained within the article.

**Acknowledgments:** The authors acknowledge financial support from the Slovenian Research Agency (Research Core Funding No. P2-0028) and the company Mahle Electric Drives Slovenia d.o.o. The authors also acknowledge Dušan Drevenshek from the Mahle Electric Drives Slovenia team for his helpful guidance.

**Conflicts of Interest:** The authors declare no conflict of interest.

## References

1. Finch, J.W.; Giaouris, D. Controlled AC Electrical Drives. *IEEE Trans. Ind. Appl.* **2008**, *55*, 481–491. [[CrossRef](#)]
2. Dementyev, Y.N.; Kojain, N.V.; Bragin, A.D.; Udut, L.S. Control system with sinusoidal PWM three-phase inverter with a frequency scalar control of induction motor. In Proceedings of the 2015 International Siberian Conference on Control and Communications (SIBICON), Omsk, Russia, 21–23 May 2015.
3. Srilad, S.; Tunyasrirut, S.; Suksri, T. Implementation of a Scalar Controlled Induction Motor Drives. In Proceedings of the 2006 SICE-ICASE International Joint Conference, Busan, Korea, 18–21 October 2006.
4. Hongyun, J.; Ming, C.; Wei, H.; Wei, L.; Xiaonfan, F. Investigation and Implementation of Control Strategies for Flux-Switching Permanent Magnet Motor Drives. In Proceedings of the 2008 IEEE Industry Applications Society Annual Meeting, Edmonton, AB, Canada, 5–9 October 2008.

5. Marchesoni, M.; Tenca, P. Diode-clamped multilevel converters: A practicable way to balance DC-link voltages. *IEEE Trans. Ind. Electron.* **2002**, *49*, 752–765. [[CrossRef](#)]
6. Nami, A.; Zare, F.; Ledwich, G.; Ghosh, A.; Blaabjerg, F. A new configuration for multilevel converters with diode clamped topology. In Proceedings of the 2007 International Power Engineering Conference (IPEC 2007), Singapore, 3–6 December 2007.
7. Rodriguez, J.; Lai, J.-S.; Peng, F.Z. Multilevel inverters: A survey of topologies, controls, and applications. *IEEE Trans. Ind. Electron.* **2002**, *49*, 724–738. [[CrossRef](#)]
8. Lin, J.; Weiss, G. Multilevel converter with variable flying capacitor voltage used for virtual infinite capacitor. In Proceedings of the 2017 International Symposium on Power Electronics, Novi Sad, Serbia, 19–21 October 2017.
9. Li, J. Design and Control Optimisation of a Novel Bypass-embedded Multilevel Multicell Inverter for Hybrid Electric Vehicle Drives. In Proceedings of the 2020 IEEE 11th Symposium on Power Electronics for Distributed Generation Systems (PEDG), Dubrovnik, Croatia, 28 September–1 October 2020.
10. Kim, H.; Jahns, T.M. Current Control for AC Motor Drives Using a Single DC-Link Current Sensor and Measurement Voltage Vectors. *IEEE Trans. Ind. Appl.* **2006**, *42*, 1539–1547. [[CrossRef](#)]
11. Matsuura, K.; Ohishi, K.; Haga, H.; Ando, I. Fine motor current control based on new current reconstruction method using one DC-link current sensor. In Proceedings of the IECON 2015—41st Annual Conference of the IEEE Industrial Electronics Society, Yokohama, Japan, 9–12 November 2015.
12. Marčetić, D.P.; Adžić, E.M. Improved Three-Phase Current Reconstruction for Induction Motor Drives with DC-Link Shunt. *IEEE Trans. Ind. Electron.* **2010**, *57*, 2454–2462. [[CrossRef](#)]
13. Single-Shunt Three-Phase Current Reconstruction Algorithm for Sensorless FOC of a PMSM. Available online: [ww1.microchip.com/downloads/en/AppNotes/01299A.pdf](http://ww1.microchip.com/downloads/en/AppNotes/01299A.pdf) (accessed on 26 May 2021).
14. 3-phase Sensorless Single-Shunt Current-Sensing PMSM Motor Control Kit with MagniV MC9S12ZVM. Available online: [www.nxp.com/docs/en/application-note/AN5327.pdf](http://www.nxp.com/docs/en/application-note/AN5327.pdf) (accessed on 26 May 2021).
15. Sensorless-FOC for PMSM with Single DC-Link Shunt. Available online: [www.ti.com/lit/an/spract7/spract7.pdf?ts=1622036373727](http://www.ti.com/lit/an/spract7/spract7.pdf?ts=1622036373727) (accessed on 26 May 2021).
16. Blaabjerg, F.; Pedersen, J.K.; Jaeger, U.; Thøgersen, P. Single current sensor technique in the DC-link of three-phase PWM-VS inverters. A review and the ultimate solution. In Proceedings of the Conference Record of the 1996 IEEE Industry Applications Conference Thirty-First IAS Annual Meeting, San Diego, CA, USA, 6–10 October 1996.
17. Blaabjerg, F.; Pedersen, J.K. An ideal PWM-VSI inverter using only one current sensor in the DC-link. In Proceedings of the 1994 Fifth International Conference on Power Electronics and Variable-Speed Drives, London, UK, 26–28 October 1994; pp. 458–464.
18. Lee, W.-C.; Lee, T.-K.; Hyun, D.-S. Comparison of single-sensor current control in the DC link for three-phase voltage-source PWM converters. *IEEE Trans. Ind. Electron.* **2001**, *48*, 491–505.
19. Shin, H.; Ha, J.I. Phase Current Reconstructions from DC-Link Currents in Three-Phase Three-Level PWM Inverters. *IEEE Trans. Power Electron.* **2014**, *29*, 582–593. [[CrossRef](#)]
20. Son, Y.; Kim, J. A Novel Phase Current Reconstruction Method for a Three-Level Neutral Point Clamped Inverter (NPC) with a Neutral Shunt Resistor. *Energies* **2018**, *11*, 2616. [[CrossRef](#)]
21. Gu, Y.; Ni, F.; Yang, D.; Liu, H. Switching-State Phase Shift Method for Three-Phase-Current Reconstruction with a Single DC-Link Current Sensor. *IEEE Trans. Ind. Electron.* **2011**, *58*, 5186–5194.
22. Ha, J.I. Voltage Injection Method for Three-Phase Current Reconstruction in PWM Inverters Using a Single Sensor. *IEEE Trans. Power Electron.* **2009**, *24*, 767–775.
23. You, J.J.; Jung, J.H.; Park, C.H.; Kim, J.M. Phase current reconstruction of three-level Neutral-Point-Clamped(NPC) inverter with a neutral shunt resistor. In Proceedings of the 2017 IEEE Applied Power Electronics Conference and Exposition (APEC), Tampa, FL, USA, 26–30 March 2017.
24. Li, X.; Dusmez, S.; Akin, B.; Rajashekara, K. A new SVPWM for the Phase Current Reconstruction of Three-Phase Three-level T-type Converters. *IEEE Trans. Power Electron.* **2015**, *62*, 2627–2637.
25. Ha, J.-I. Current Prediction in Vector-Controlled PWM Inverters Using Single DC-Link Current Sensor. *IEEE Trans. Ind. Electron.* **2009**, *57*, 716–726.
26. Lai, Y.S.; Lin, Y.K.; Chen, C.W. New Hybrid Pulsewidth Modulation Technique to Reduce Current Distortion and Extend Current Reconstruction Range for a Three-Phase Inverter Using Only DC-link Sensor. *IEEE Trans. Power Electron.* **2013**, *28*, 1331–1337. [[CrossRef](#)]
27. Cho, Y.; LaBella, T.; Lai, J.-S. A Three-Phase Current Reconstruction Strategy With Online Current Offset Compensation Using a Single Current Sensor. *IEEE Trans. Ind. Electron.* **2012**, *59*, 2924–2933. [[CrossRef](#)]
28. Lu, H.; Cheng, X.; Qu, W.; Sheng, S.; Li, Y.; Wang, Z. A Three-Phase Current Reconstruction Technique Using Single DC Current Sensor Based on TSPWM. *IEEE Trans. Power Electron.* **2014**, *29*, 1542–1550.
29. Current Sensing. Available online: [kappaiq.com/download/presentation-material/PDF/04%20Current%20Sensing.pdf](http://kappaiq.com/download/presentation-material/PDF/04%20Current%20Sensing.pdf) (accessed on 26 May 2021).
30. Yan, H.; Xu, Y.; Zhao, W.; Zhang, H.; Gerada, C. DC Drift Error Mitigation Method for Three-Phase Current Reconstruction with Single Hall Current Sensor. *IEEE Trans. Magn.* **2018**, *55*, 1–4. [[CrossRef](#)]